TO MY HUSBAND and MY PARENTS

FT-IR SPECTROSCOPIC CHARACTERIZATION of the INTERMEDIATES in the SELECTİVE CATALYTIC REDUCTION of NO WITH METHANE on Pd/ZrO_2-WO_x CATALYST

A THESIS
SUBMITTED TO THE DEPARTMENT OF CHEMISTRY
THE INSTITUTE OF ENGINEERING AND SCIENCES OF
BILKENT UNIVERSITY
IN PARTIAL FULFILLMENT OF THE REQUIREMENTS
FOR THE DEGREE
OF
MASTER OF SCIENCE

By
İLKNUR ÇAYIRTEPE

SEPTEMBER 2004

I certify that I have read this thesis and in my opinion it is fully adequate, in scope and quality, as a thesis of the degree of Master of Science

_____

Assoc. Prof. Margarita Kantcheva (Supervisor)

I certify that I have read this thesis and in my opinion it is fully adequate, in scope and quality, as a thesis of the degree of Master of Science

_____

Prof. Dr. Şefik Süzer

I certify that I have read this thesis and in my opinion it is fully adequate, in scope and quality, as a thesis of the degree of Master of Science

_____

Assoc. Prof. Ömer Dağ

I certify that I have read this thesis and in my opinion it is fully adequate, in scope and quality, as a thesis of the degree of Master of Science

_____

Assoc. Prof. Gürkan Karakaş

I certify that I have read this this thesis and in my opinion it is fully adequate, in scope and quality, as a thesis of the degree of Master of Science

_____

Assoc. Prof. Deniz Üner

Approved for the Institute of Engineering and Sciences

_____

Prof. Dr. Mehmet Baray

Director of Institute of Engineering and Sciences

ABSTRACT

FT-IR SPECTROSCOPIC CHARACTERIZATION of the INTERMEDIATES in the SELECTİVE CATALTIC REDUCTION of NO WITH METHANE on Pd/ZrO_2-WO_x CATALYST

İLKNUR ÇAYIRTEPE

M.S. in Chemistry

Supervisor: Assoc. Prof. Margarita Kantcheva

September 2004

This work involves in situ FT-IR spectroscopic study of the routes of formation, composition and thermal stability of strongly bound NO_x complexes on the surface of Pd/tungstated zirconia, and transformation of the surface NO_x complexes in the presence of methane in order to elucidate the mechanism of selective catalytic reduction of NO with methane. Sol-gel polymer-template synthesis was chosen to obtain high surface area in the preparation of the tungstated zirconia used as support (WO_3 nominal content of 18.6 wt %). The Pd(II) ions (0.1 wt%) have been deposited by impregnation. PXRD characterization shows that the support and the catalyst are tetragonal and contain mesoporous phase.

The adsorption of NO at room temperature on the tungstated zirconia shows presence of coordinatively unsaturated Zr(IV) ions. The spectrum of NO adsorbed on palladium modified on tungstated zirconia reveals the existence of two types of Pd(II) sites. No exposed Zr(IV) ions are observed. The surface NO_x species (N_2O_3, nitro and nitrito ions) on both samples are produced at room temperature by oxidation of NO with the W^{6+}=O species. In the case of the Pd/tungstated zirconia, palladium(II) can oxidize NO to NO_2 at 623 K.

The adsorption of NO/O_2 mixture at room temperature on the samples studied leads to formation of various kinds of surface nitrates characterized by different modes of coordination. The thermal stability of the nitrate species formed on both samples is comparable: They disappear after dynamic evacuation at 673 K. However, lower concentration of the surface nitrates on the Pd/tungstated zirconia compared to that on the tungstated zirconia indicates that in the former case the nitrates are coordinated to the support.

The experimental results show that methane interacts differently with the NO_x-precovered tungstated zirconia and Pd/tungstated zirconia although both materials are able to activate methane at the same temperature in absence of adsorbed NO_x species. In the case of the tungstated zirconia the surface nitrates suppress the oxidation of methane, whereas the NO_x-precovered Pd/tungstated zirconia catalyzes the formation of nitromethane. The latter compound is considered as a key intermediate in the selective catalytic reduction of NO with methane in excess oxygen. A mechanism, which involves direct activation of methane by the catalyst, leading to the products of the selective reduction (N_2, CO_2 and H_2O) is proposed.

Keywords: Adsorption of NO and NO/O_2; In situ FT-IR spectroscopy; tungstated zirconia; Pd supported on tungstated zirconia; NO selective catalytic reduction by methane; Mechanism; Nitromethane.

ÖZET

Pd/ZrO_2-WO_x KATALİZÖR ÜZERİNDE METHANE ile SEÇİCİ KATALİTİK İNDİRGENMEDE OLUŞAN ARA ÜRÜNLERİN FT-IR SPEKTROSKOPİK KARAKTERİZASYONU

İLKNUR ÇAYIRTEPE
Kimya Bölümü Yüksek Lisans
Tez Yöneticisi: Assoc. Prof. Margarita Kantcheva
September 2004

Bu çalışma metan ile NO'nun seçici katalitik indirgenme mekanizmasını açıklamak için Pd/tungstenlenmiş zirkonyum yüzeyinde kuvvetlice bağlanmış NO_x komplekslerinin methane varlığında oluşmasının, kompozisyonun ve termal kararlılığının *in-situ* FT-IR spektroskopik çalışmasını içermektedir. Yüzey alanını geniş elde etmek için tungstenlenmiş zirkonyumun (ağırlıkça18.6 % WO_3 nominal içerikli) hazırlanmasında Sol-gel polimer-template sentezi seçilmiştir. İmpregnasyon yöntemi kullanılarak Pd(II) iyonları (ağırlıkça 0.1%) depolanmıştır. PXRD karakterizasyonu katalizörün tetragonal ve mesoporus fazlarını içerdiğini göstermiştir.

Tungstenlenmiş zirkonyum üzerine oda sıcaklığında NO adsorpsiyonu koordinasyona açık Zr^{4+} iyonlarının olduğunu göstermiştir. Pd içeren numunenin NO adsorpsiyonu iki çeşit Pd(II)'nin bulunduğunu açığa çıkarmış ve koordinasyona açık Zr^{4+} iyonları gözlenmemiştir. İki numune üzerindeki NO_x türleri (N_2O_3, nitro and nitrito iyonları) oda sıcaklığında NO'nun W^{6+}=O gruplarıyla oksitlenmesi sonucu üretilmiştir. Pd/tungstenlenmiş zirkonyum üzerinde paladyum(II) 623 K de NO'yu NO_2'ye oksitleyebilmektedir.

NO ve O_2 karışımının oda sıcaklığında, çalışılan numunelere adsorpsiyonu, koordinasyonları farklı olan çeşitli yüzey nitratlarının oluşmasını

sağlamıştır.Her iki numunede de oluşan nitratların termal kararlılıkları benzerdir. 673 K deki dinamik vakumlama sonrasında nitratlar yok olmuşlardır. Bununla beraber Pd/tungstenlenmiş zirkonyum üzerinde oluşan yüzey nitratlarının düşük konsantrasyonu, nitratların tungstenlenmiş zirkonyuma koordinasyonunu belirtmektedir.

Adsorbe olmuş NO_x türlerinin yokluğunda iki numune de hidrokarbonu aynı sıcaklıkta aktifleştirmiş olmasına rağmen, deneysel sonuçlar metanın NO_x ile daha önce kaplanmış tungstenlenmiş zirkonyum ve Pd/tungstenlenmiş zirkonyumun farklı şekillerde etkileştiğini göstermiştir. Tungstenmiş zirkonyumda yüzey nitratları metanın oksidasyonunu bastırırken, NO_x ile daha önce kaplanmış Pd/tungstenlenmiş zirkonyum nitrometan oluşmasını katalizlemektedir. Nitrometan, NO'nun metan ile seçici katalitik indirgenmesinde anahtar ara ürün olarak düşünülmektedir. Hidrokarbonun direk activasyonunu içeren ve seçici indirgenme ürünlerini (N_2, CO_2 and H_2O) oluşturan bir mekanizma önerilmiştir.

Anahtar Kelimeler: NO and NO/O_2 adsorpsiyonu; *in-situ* FT-IR specktroskopi; tungstenlenmiş zirconyum; Pd depolanmış tungstenlenmiş zirconyum; NO'nu metan ile seçici katalitik indirgenmesi; Mekanizma; Nitrometan.

ACKNOWLEGMENT

It is a pleasure for me to express my deepest gratitude to Dr. Margarita Kantcheva for her encouragement and supervision throughout my studies.

I would to thank to Olga Samarskaya and Tuğba Arzu Özal for their precious help and moral support.

I would like to thank all present and former members of Bilkent University Chemistry Department for their help.

I would like to express my deepest gratitude to my husband Fatih Çayırtepe for endless support and love.

TABLE OF CONTENTS

LIST OF TABLES

LİST OF FIGURES

1. INTRODUCTION

1.1. General about the Selective Catalytic Reduction of NO_x

Fossil fuels are combusted in transport devices, power plants, house heating and the chemical industry. Since the concept is almost the same for each application, transport devices are exemplified in order to explain how undesirable gases are produced.

Power is supplied to the majority of automobiles and trucks by a spark ignited gasoline engine. Gasoline is a mixture of paraffins and aromatic hydrocarbons, which combust in air very efficiently. In the engine the following ideal combustion reaction is considered to take place:

$$\text{Petrol} + O_2 \text{ (in air)} \rightarrow CO_2 + H_2O + \text{Heat}$$

In addition to these products, carbon monoxide (CO), unburned hydrocarbons (HC), nitrogen oxides (NO_x), hydrogen (H_2) and oxygen (O_2) can be identified in exhaust gases [1]. NO_x, CO and HC are the primary atmospheric pollutants. CO poisons human-beings. HC is a potential greenhouse gas. Reaction between HC and NO_x, which is enhanced by sunlight, leads to the formation of ground level ozone. NO_x particularly has the ability to cause the formation of photochemical smog, acid rain and airborne particulate, through ammonium nitrate formation [1,2,3].

Because of the environmental reasons, in automobile exhaust gases CO and HC should be oxidized to CO_2 and H_2O meanwhile NO_x should be reduced to the desired product N_2. The oxidation reactions are:

$$C_xH_n + (x+n/4)\ O_2 \rightarrow xCO_2 + (n/2)\ H_2O$$

$$2CO + O_2 \rightarrow 2CO_2$$

And the reduction reactions are:

$$2NO + 2CO \rightarrow N_2 + 2CO_2$$

$$2NO + H_2 \rightarrow N_2 + H_2O$$

$$(2x+n/2)\ NO + C_xH_n \rightarrow (x+n/4)\ N_2 + xCO_2 + (n/2)\ H_2O$$

New automobile technology requires catalysts, which cause above reactions to occur at lower temperatures. Since the catalyst simultaneously promotes these reactions, it is called *the three-way catalyst* (TWC). The catalytic performance of the three-way catalyst is a function of the engine air to fuel ratio (Fig.1). The best performance of TWC is obtained at the air-fuel ratio of 14.6:1. So non-selective reduction of NO_x is accomplished by HC, CO and/or H_2. Thus, the primary pollutants in the exhaust gases are converted to desired chemical products [1,2,3].

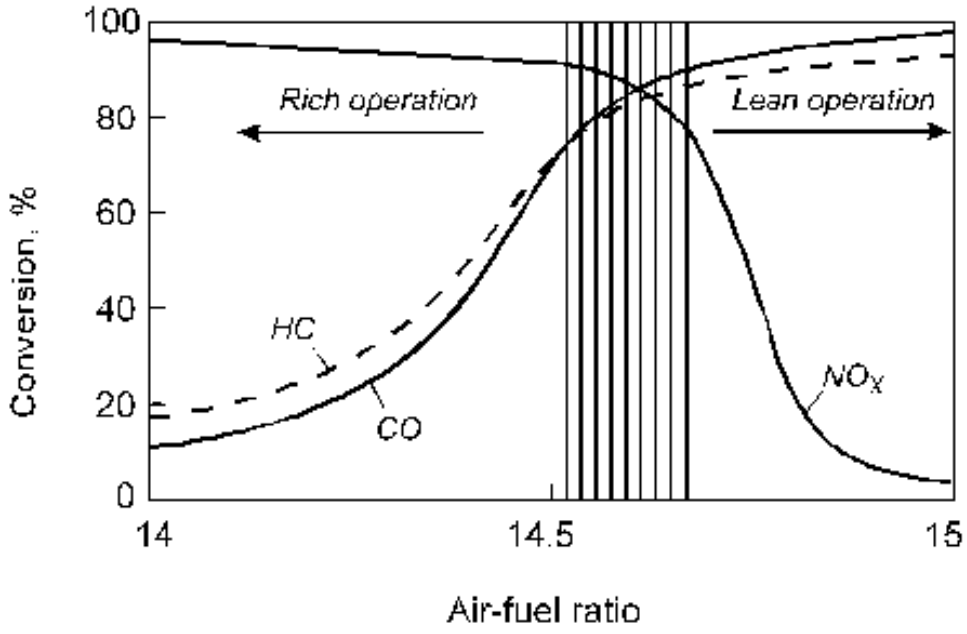

Figure 1. The conversion efficiency (%) of a three-way catalyst as a function of A/F-ratio. The lambda window, an A/F-ratio of 14.6 corresponds to stoichiometric operation, $\lambda = 1$ [4].

The TWC is inefficient to reduce NO_x for the lean-burn engine applications ($\lambda > 1$), e.g. diesel engines and lean burn gasoline engines. The NO_x reduction by HC under the excess oxygen condition is called *selective catalytic reduction* (SCR), in which the reductant intentionally reacts with nitrogen oxides instead of being burned by oxygen [1,5,6]:

$$2NO_x + C_zH_y + (z\text{-}x+y/4)\ O_2 \rightarrow N_2 + zCO_2 + (y/2)\ H_2O$$

1.2. Selective Catalytic Reduction by Methane – What is the advantage?

Industrial sources of NO_x are from stationary plants, which are coal- and oil-fired power plants, incinerators and gas turbines. NO_x is currently removed from exhaust streams in lean burn conditions and at lower temperature by the selective catalytic reduction with ammonia. A conventional SCR system is shown in Fig. 2 [7].

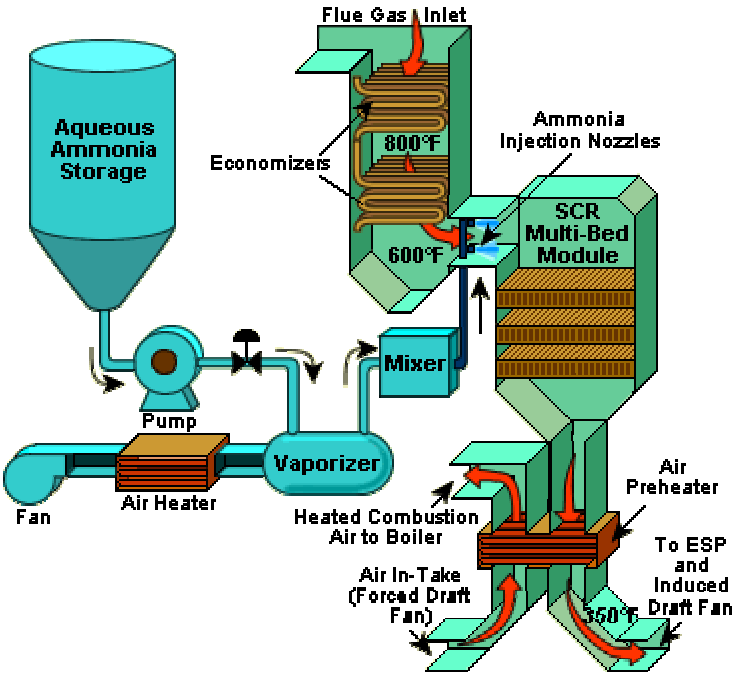

Figure 2. Example SCR System for NO_x control in a boiler.

In SCR systems, ammonia vapor is used as the reducing agent and is injected into the flue gas stream, passing over a catalyst. The SCR with ammonia breaks down nitrogen oxide to form molecular nitrogen and water with the following reactions [8];

$$4NO + 4NH_3 + O_2 \rightarrow 4N_2 + 6H_2O$$

$$2NO_2 + 4NH_3 + O_2 \rightarrow 3N_2 + 6H_2O$$

NO_x emission reductions over 80-90% can be achieved and the optimum temperature is usually between 300°C and 400°C, which is normally the flue gas temperature at the economizer outlet. The V_2O_5 loaded on TiO_2, which is

further doped by manganese or molybdenum oxides, is the most used catalyst in the coal-fired plants. Yet there are other catalysts used industrially, which are activated carbon or platinum.

Even though SCR by NH_3 is a very promising technology in terms of efficiency and sulfur tolerance, it has some drawbacks at the same time. The toxicity is the main drawback in the use of ammonia and then precautions have to be taken during storage and transportation. The SCR with NH_3 produces relatively high N_2O emissions compared to a conventional diesel engine. The amount of ammonia injected into the SCR is critical to its successful operation. If too little ammonia is injected, some of the NO_x will not be converted and if too much ammonia is injected, some of the ammonia will "slip" past the catalyst and become a new emission problem. So the ammonia slip in SCR processes should be minimized that supposes an optimization of the ammonia feed. Finally, accumulation of ammonium sulfates can induce significant pressure drops and/or further corrosion phenomena, which alter the efficiency of SCR processes. Therefore this SCR with NH_3 requires high capital investment, infrastructure development and operational cost [3,5].

Presently, the use of hydrogen or hydrocarbon, mainly methane, could be an alternative, which offers new perspective in the utilization of natural gas. Selective catalytic reduction with hydrocarbons (SCR-HC) is expected to be a more convenient and cheaper alternative. In this respect, particularly the use of methane, readily available as natural gas, already in use as fuel and not corrosive, is very attractive. It also removes the storage problem. Furthermore, the slippage of hydrocarbon is more environmentally benign than ammonia, although it is still necessary to minimize the slippage. Thus, the use of methane offers the opportunity for significantly reduced capital and operating costs [10]. The selective catalytic reduction of NO_x with methane is according to the following reaction:

$$2NO + CH_4 + O_2 \rightarrow N_2 + CO_2 + 2H_2O$$

The most possible applications of this technology using methane as a reducing agent are for exhaust from natural gas-fired power plants and lean-burn natural–gas engines. The catalyst for mobile applications should have high activity and exceptional durability. The catalyst, which is candidate for the industrial power plants, should not be poisoned from water vapor and SO_2.

Zeolite-based catalysts (e.g. Co-, Ga-, In-ZSM-5) can be particularly effective [3,11-16]. However, their NO_x reduction activity and durability is deteriorated when exposed to wet reaction conditions [3,12,14,16]. Use of simple oxide support with strong surface acidity provides an alternative approach to achieve better performance of the catalysts for the selective catalytic reduction of NO with methane in moist streams. The most promising materials as catalysts are supported metal oxides (e.g. Pd/TiO_2, Pt/Al_2O_3, Pd/WO_x-ZrO_2,...) [17-19]. They exhibit activity comparable to the zeolitic catalyst in the SCR of NO_x by CH_4. Unlike zeolitic catalysts, supported noble metal oxides are much more stable hydrothermally. Furthermore, flexibility in the preparation of mixed metal oxides with a desired composition puts importance for practical catalysts [20].

1.3. Main Characteristics of Tungstated Zirconia as a Support

Acidity is the important phenomenon in oxide supports for the selective catalytic reduction of NO_x with methane since the acidity of the support determines the activity toward CH_4 in the absence of zeolitic structure [20,21]. Acidity of the supports can be modified by choosing the appropriate synthesis techniques, doping with transition and/or non-transition oxides and adjusting the amount of modifiers.

Zirconia has taken interest as a support [18,22-26] due to the amphoteric properties [27]. Stable monoclinic and metastable tetragonal phases can be intentionally obtained by using various preparation routes, which have different starting raw materials and different pretreatment conditions, and by adding tiny amount of impurities [28-34]. Zhao et al. [35] reported that tetragonal zirconia has only Lewis acid sites on the surface but monoclinic zirconia has both Brønsted and Lewis acid sites. Bolis et al. [36] stated that Lewis acidic sites on the surfaces of tetragonal zirconia are much stronger than those on the surfaces of monoclinic zirconia even though the Lewis acid sites are more abundant on monoclinic zirconia. The acidity of the zirconia can be changed by doping with sulfate ions and tungsten oxide, both of which enhance the acidity. Whereas sulfated zirconia shows more acidic character than tungstated zirconia [36-38], sulfated zirconia suffers from rapid deactivation, sulfur loss during reaction

conditions and regeneration. Thus, tungstated zirconia has taken more attention as a strong solid acid.

It has been reported that WO_3 supported on ZrO_2 exhibits strong Brønsted and Lewis acidity when WO_3 covered the ZrO_2 surface as a monolayer [39-42]. Additionally, the preparation method involving simultaneous coprecipitation of tungsten with the formation of hydrous zirconia results in a catalyst and/or a support with increased strong acid site density as compared to the catalyst and/or the support prepared by tungsten impregnation of hydrous and calcined zirconia [43-46]. Chin et al. [18] observed that tungstated zirconia as a support of a $DeNO_x$ catalyst is more tolerant to water vapor because of the simple structure and shows resistance to SO_2 poisoning.

In order to increase the activity and selectivity toward the reduction of NO with methane Pd is deposited on the tungstated zirconia [18,19,47].

1.4. Mechanism of Selective Catalytic Reduction of NO_x on Pd-containing Catalysts

Lobree et al. [48] proposed a reaction mechanism for the reduction of NO with CH_4 by using mass spectroscopy and in-situ infrared spectroscopy. They observed that the reduction of NO by CH_4 started by the interaction of methane with the adsorbed NO above 650 K, which produces CH_2NO (or its isomer CHNOH) in the form of $Z^-H^+[Pd(H)(CH_2NO)]^+Z^-$ species. CH_2NO decomposes to produce water and highly reactive neutral CN species ($Z^-H^+[Pd(H)(CN)]^+Z^-$) as intermediates, which further react with NO or O_2 (if present). Reaction with NO forms N_2 and CO, whereas reaction with O_2 yields NO and CO. For this process the principal active component in Pd-H-ZSM-5 is found to be Pd^{2+}.

Shimizu et al. [49] investigated the mechanism of NO reduction by methane in the presence of O_2 over Pd-H-Mordenite. They concluded from in-situ UV-Vis, in-situ IR data and kinetic results that CH_4-derived reactive species reduces the adsorbed NO on Pd^{2+} in order to produce NH_4^+ on the zeolite acid sites. The formed NH_4^+ reacts with Pd^{2+}-nitrosyl and NO_2 species, which results in the desired product N_2. They also believe that Pd^{2+}-NO and NH_4^+ are the possible key intermediates for this reaction mechanism and isolated Pd^{2+} ions and

Brønsted acid sites are indispensable for intermediates. And the kinetic results confirm the proposed mechanism.

Lukyanov et al. [50] stated from kinetic studies that interaction of methane with adsorbed NO_2 initiated the catalytic reduction of NO_x into N_2 and oxidation of CH_4. The intermediate species, CH_3•, was formed due to H abstraction of NO_2 since NO_2 is a free radical and stronger oxidizing agent than NO.

Mechanistic study on titania-supported palladium pointed out NH_3 as an intermediate [17,51]. Ozkan et al. observed that the linearly adsorbed NO on metallic Pd disappeared upon methane addition and NH_3 adsorbed on Lewis acid sites has been formed. They proposed that methane was activated on Pd^o sites.

Sun et al. [52] suggested nitromethane as an intermediate in the reduction of NO over Co^{2+} modified ZSM-5 catalysts. In the oxidizing atmosphere NO easily interacts with Co-ZSM-5, resulting in the formation of adsorbed NO_2 species. And methane reacts with adsorbed NO_2 to produce nitromethane intermediate, which further reacts with NO_2 to yield N_2, H_2O and CO_2.

If nitromethane is observed as an intermediate in the selective catalytic reduction of NO with CH_4, isocyanide (NCO), hydrogen cyanide (HCN), ammonia (NH_3), carbamic acid, nitrous oxide (N_2O), cyanuric acid (HNCO), melamine can be detected as decomposition products/intermediates [53-57].

The temperature dependence of NO conversion to nitrogen with various hydrocarbons in excess oxygen (Fig. 3) displays a volcano shape [58]. This indicates that strongly bound NO_x surface complexes are involved in the selective conversion of NO to molecular nitrogen in excess oxygen.

The aims of this study are:

(i) to determine by means of in situ FT-IR spectroscopy routes of formation, composition and thermal stability of strongly bound NO_x complexes on the surface of Pd/tungstated zirconia, and

(ii) to investigate transformation of surface NO_x complexes in the presence of methane in order to elucidate the reaction mechanism.

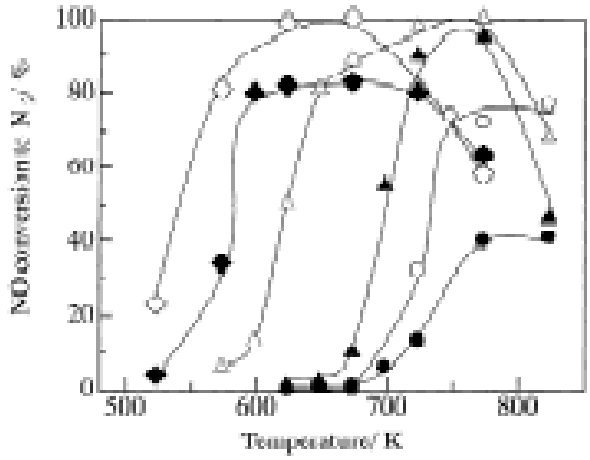

Figure 3. NO conversion to nitrogen on Ag/Al_2O_3 using various n-alkanes: (●) methane, (○) ethane, (▲) propane, (△) butane, (✧) hexane, (✦) octane. Conditions: NO = 1000 ppm, alkane = 6000 ppm,, O_2 = 10 %, H_2O = 2 %, and W/F = 0.12 g.s/cm^3, except for methane-SCR (W/F = 0.9 gs/cm^3) [58]

1.5. Identification of adsorbed NO_x species by FT-IR Spectroscopy

Adsorptions of NO and its coadsorption with O_2 lead to formation adsorbed NO_x species, whose identifications are important for the mechanistic study of selective catalytic reduction of NO.

The negatively charged species usually observed on the surface of the catalysts are nitrite (NO_2^-) and nitrate (NO_3^-) anions. The free nitrite anion has a C_s symmetry and absorption bands due to $\nu_{as}(NO_2)$ and $\nu_s(NO_2)$ modes are at 1330 and 1260 cm^{-1}, respectively [59]. When NO_2^- is coordinated by one or two of its oxygen atoms, nitrito species are formed. When NO_2^- is coordinated by its nitrogen atom, nitro compounds are formed. Characteristic IR regions for nitro/nitrito compounds are given in Table 1.

The free nitrate is planar and has a D_{3h} symmetry. It shows three IR active modes: asymmetric stretching (ν_3) at 1430 cm^{-1}, out-of-bending (ν_2) at 825 cm^{-1} and in-plane-bending (ν_4) at 722 cm^{-1} [60]. ν_1 is symmetric and is only observed in Raman spectra. After coordination, ν_1 becomes IR active and the degeneracy of ν_3 is removed so that ν_3 splits into two components. The magnitude

of the splitting depends on the coordination type of the nitrates. The absorption ranges for nitrates are presented in Table 1.

The IR absorption bands for nitrite and nitrates sometimes overlap in the 1350-1550 cm^{-1} region. In that case, combination bands of nitrates can be used for structural identification. The combination bands of the bridged nitrates are at 2845-2800 cm^{-1} [ν_s(N=O) + ν_s(NO_2)] and pair bands at 1980-1960 [ν_s(NO_2) + δ(ONO)] and 1900-1890 cm^{-1}[ν_s(NO_2) + δ(ONO)]. Bidentate nitrates produce combination bands in the region of 2600 cm^{-1} [ν_s(N=O) + ν_s(NO_2)] and pair of bands at 1755 and 1700 cm^{-1} [ν_s(NO_2) + δ(ONO)] [60].

Stability of adsorbed NO_x species can give information about their nature. The noncharged species, e.g. NO, $(NO)_2$, NO_2, N_2O_3 and N_2O_4, are generally weakly adsorbed and easily removed from the surface upon evacuation at room temperature. But charged species, e.g. NO^+, NO_2^-, NO_3^-, NO^- are stable. They need to be heated at elevated temperatures in order to desorp from the surface. The nitro species are more stable than the nitrito species and bridged and bidentate nitrates are more thermally stable than the monodentate nitrates.

Table 1: Spectral characteristics of NO_x species observed on the metal oxides [59,60,62,63]

NO_x Species	Vibration Modes	Wavenumbers (cm^{-1})
Free nitrite ion, NO_2^-	$\nu_{as}(NO_2)$ $\nu_s(NO_2)$ $\delta(ONO)$	1250 1335 830
Nitro, M-NO_2	$\nu_{as}(NO_2)$ $\nu_s(NO_2)$ $\delta(ONO)$	1370-1470 1320-1340 820-850
Nitrito, M-O-NO	$\nu(N=O)$ $\nu(NO)$ $\delta(ONO)$	1400-1485 1050-1100 820-840
Chelated Nitrito, (M-O_2)=N	$\nu_{as}(NO_2)$ $\nu_s(NO_2)$ $\delta(ONO)$	1270-1390 1170-1225 840-860
Bridging nitro, M-O-N(O)-M	$\nu_{as}(NO_2)$ $\nu_s(NO_2)$	1390-1520 1180-1260
Bidentate nitro	$\nu_{as}(NO_2)$ $\nu_s(NO_2)$	1390-1520 1180-1260
Free nitrate ion, NO_3^-	$\nu_{as}(NO_2)$	1430
Monodentate nitrate, M-O-NO_2	$\nu_{as}(NO_2)$ $\nu_s(NO_2)$ $\nu(NO)$	1450-1570 1250-1330 970-1035
Bidentate nitrate, M-O_2NO	$\nu_{as}(NO_2)$ $\nu_s(NO_2)$ $\nu(NO)$	1200-1310 1003-1040 1500-1620
Bridged nitrate, (M-$O)_2$=NO	$\nu_{as}(NO_2)$ $\nu_s(NO_2)$ $\nu(NO)$	1200-1260 1000-1030 1590-1660

2. EXPERIMENTAL

2.1. Sample Preparation

2. 1. 1. Tungstated zirconia

The mesoporous tungstated zirconia was synthesized by using polyvinyl alcohol (PVA) as a template [34]. The following procedure was applied; 30 g of $ZrOCl_2.8H_2O$ was dissolved in 150 ml of H_2O. 2.6 ml of 0.4 M ammonium metatungstate solution was added to zirconium oxychloride solution while stirring. The mixed solution was heated up to 100ºC in a water bath and kept for 1 h at this temperature. Besides, the aqueous solution of PVA was prepared by dissolving 15 g of PVA in 150 ml of H_2O (on heating). The hot solutions of PVA and zirconium tungstate were mixed and kept for 1 h at 100ºC, then cooled to 60ºC. The colloidal solution was poured into a prepared buffer solution (NH_4Cl + NH_4OH) under stirring. Granules of a transparent elastic gel were formed. And the obtained mixture stayed for 1 h at room temperature while stirring. Then it was washed with distilled water several times until the disappearance of chlorine anions in the washing water. The washed gel was dried in a drying oven at 373 K whereupon the transparent gel was heated up to 473 K and kept at this temperature for 24 h in air. Then the sample was placed into a quartz tube and heated slowly under vacuum up to 673 K. It stayed for 2 h at this temperature. Afterwards, the sample was heated up to the final carbonization temperature of 923 K and let to stand for 2h at this temperature. The obtained sample was calcined for 5 h at 773 K in air to burn the carbon-containing compounds. The black carbonized sample was completely white after ~30 minute (see flow chart 1).

The finally obtained tungstated zirconia sample was heat treated initially at 873 K then at 973 K for 1 h in order to follow the behavior of mesoporous phase. The nominal content of WO_3 is 18.6 wt %.

Flow Chart 1 for the preparation of the WZ:

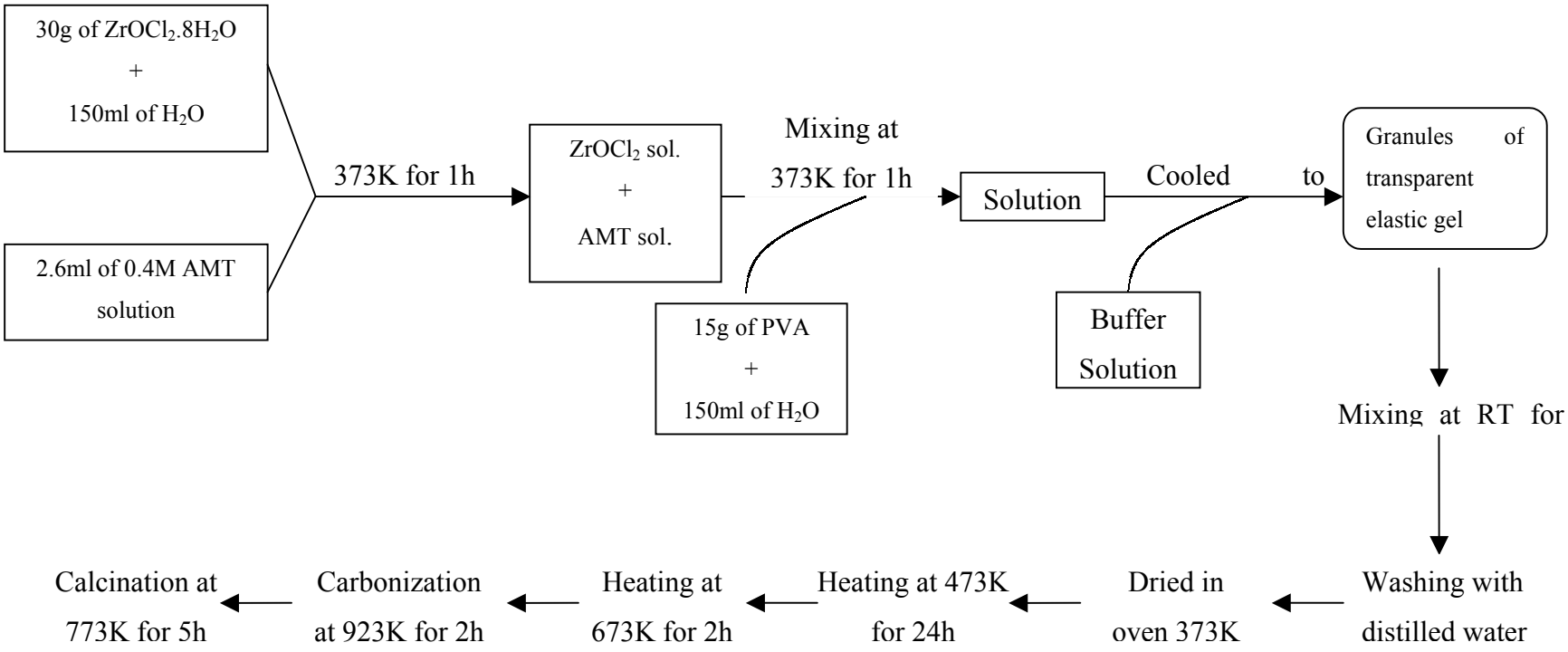

This method is preferred to prepare the tungstated zirconia sample because:

- Simultaneous coprecipitation of tungsten with the formation of hydrous zirconia produces a material with increased strong acid site density,
- High surface area can be obtained due to the presence of the mesoporous phase,
- WO_3 can cover the ZrO_2 surface as a monolayer,
- Growing of ZrO_2 crystals can be retarded due to pinning effect of WO_3 and mesoporous phases.

In this synthesizing method, PVA acts as a templating agent in the coprecipitation of tungsten and hydrous zirconia and can remain in the material up to temperatures of 600-700ºC. So the crystallization of the zirconia occurs without a collapse of the mesoporous structure during the carbonization step. The residue of PVA after carbonization can be removed easily in the oxidizing atmosphere at lower temperature (500ºC).

The tungstated zirconia notations used further in the text are summarized in Table 2.

Table 2: Tungstated zirconia sample notations

Sample	Treatment
WZ200	After drying the precipitate at 200^0C for 24 h in air
WZ400	After heating in vacuum at 400^0C for 2 h
WZ650	After heating in vacuum at 650^0C for 2 h
WZ	After calcination at 500^0C for 5 h
WZ600HT	After heating at 600^0C for 1 h
WZ700HT	After heating at 700^0C for 1 h

2. 1. 2. Zirconia

The mesoporous zirconia was synthesized just like in the case of the mesoporous tungstated zirconia but without using tungstate and the final carbonization temperature was chosen as 873 K.

The pure zirconia notations used further in the text are summarized in Table 3.

Table 3: Pure zirconia sample notations

Sample	Treatment
Z200	After drying the precipitate at 200^0C for 24 h in air
Z400	After heating in vacuum at 400^0C for 2 h
Z600	After heating in vacuum at 600^0C for 2 h
Z	After calcination at 500^0C for 5 h

2. 1. 3. Palladium Modified Tungstated Zirconia

Palladium nitrate is used as a source of Pd^{2+} ions. 0.001 M Pd^{2+} solution was prepared for the synthesis of 0.10% Pd on tungstated zirconia. 1.5 g of WZ was impregnated with 14.1 ml of 0.001 M Pd^{2+} solution. The impregnated samples were dried by stirring at mild heating. Then it was calcined at 773 K for 5 hours.

Pd/WZ notation for palladium modified tungstated zirconia is used further in the text.

2. 2. Surface Area Measurements and XRD

The BET surface area of the samples was measured by nitrogen adsorption at 77 K by using a MONOSORP apparatus from Quantachrome. Before the measurements, the samples were dehydrated at 573 K for 1 hour.

XRD analysis was performed on a Rigaku Miniflex diffractometer with Ni-filtered Cu K_α radiation at ambient conditions. The scan speed was 1º/min.

2. 3. IR Spectroscopy

The FT-IR spectra were recorded on a Bomem MB 102 FT-IR (Hartman & Braun) spectrometer equipped with a liquid-nitrogen cooled MCT detector at resolution of 4 cm^{-1} (128 scans).

2. 3. 1. Experimental Setup

Two different types of IR cell were used in the experiments. One of the IR cell equipped with NaCl windows allowed the activation of the sample at high temperatures and the recording of the spectra at ambient temperature. The other type of the IR cell (Xenonum Scientific SVCS, USA) allowed recording of the spectra at ambient and elevated temperatures (with BaF_2 windows). The sample holder of the cell can be moved up and down relatively to the light beam, which gives the possibility for the subtraction of the gas phase spectrum when needed. . The IR cell is connected to a vacuum/adsorption apparatus.

2. 3. 2. Activation of the Samples

Self-supporting discs (0.040 g/cm^2) were used for the FT-IR studies. The pressed Pd/WZ sample was activated by heating for 1 h in vacuum at 723 K and in oxygen (13.3 kPa) at the same temperature followed by evacuation for 1 h at that temperature. The pressed WZ sample was activated by heating for 1 h in vacuum at 723 K and in oxygen (13.3 kPa) at the same temperature followed by evacuation for 1 h at 573 K.

The spectra of the activated sample were taken at high temperature and room temperature, which were used as background references. The spectra of the samples that were subjected to heat treatments at elevated temperatures were recorded at those temperatures. The high temperature background reference was used in the subtraction of the spectra taken at high temperatures and correspondingly the room temperature background reference was used for the spectra registered below 423 K.

When the experiment were performed at high temperatures, changes in the OH region could not detected because the water vapor (if produced) adsorbed dissociatively on the BaF_2 windows, which were cooled by running water.

2. 3. 3. Adsorption of NO and NO/O_2

99.9 % (Air products) purity of NO was used. NO adsorption was conducted at room temperature with the introduction of 1.33 kPa of NO and the evolutions of the IR spectra with time were taken.

Co-adsorption of NO and O_2 was accomplished at room temperature with the introduction of gas mixture (1:2) of NO and O_2 for a given period of time.

The thermal stability of the created NO_x species was tested by heating the catalyst for 15 or 20 min under vacuum in the temperature range 473-723 K.

2. 3. 4. Interaction of the CH_4 with the Catalysts

8 kPa of methane was added into the IR cell in order to observe the interaction of CH_4 with the catalyst. Then, the closed cell was heated from 523K to 723 K and the samples were allowed to stay for 20 min at each temperature level.

2. 3. 5. Interaction of the Methane with the NO_x-precovered catalysts

After the formation of NO_x species by room temperature adsorption of NO and O_2 (1:2) followed by evacuation for 15 min, 7.33 kPa of CH_4 was added. The interaction of the methane with the NO_x-precovered catalyst was observed in the temperature range 523 – 723 K. The interaction time was chosen 15 or 20 min for each temperature level.

3. RESULTS AND DISCUSSION

3. 1. Characterization of the Samples

3. 1. 1. BET Surface Area Measurements and XRD

Table 4: BET surface areas of the samples

Sample	BET surface area [m^2/g]
ZrO_2	153
WZ	210

3. 1. 1. 1. Tungstated zirconia

X-ray diffraction pattern of the heated sample at 673 K, denoted by WZ 400, shows one sharp peak at 2.9º and two broad features in the range of 2θ from 20 to 38º and from 40 to 70º (Fig. 4). The broad peaks indicate a very low degree of crystallinity. Existence of mesoporous phase in the sample can be determined from the sharp peak at low angle [64].

The diffractogram of the carbonized sample at 923 K, designated by WZ 650, reveals that it consists of crystalline tetragonal zirconia phase and randomly distributed mesoporous phase.

The size of crystallites was calculated by the use of the Scherrer's equation [65]:

$$t = 0.9\lambda / (B*\cos\theta_B)$$

where λ is the wavelength of the X-Ray, B is the full with at half maximum (in radian) of the reflection, θ_B is the position of the reflection in the XRD pattern and t is the crystal size. Not only the crystallite size causes the broadening of the reflection peak but also the instrumental broadening causes. Slit widths, sample size, penetration in the sample, imperfect focusing and unresolved α_1 and α_2 peaks of the source are the reason of the instrumental broadening. Instrumental peak broadening can be determined by using a very big crystal of the sample. Since crystal size effect on the peak broadening is removed due to the large crystallite

size of the sample, the full with at half maximum of the reflection band comes from the instrumental sources. So the peak broadening due to instrumental sources is removed. Si sample with 2000 nm crystallite size was used in order to determine instrumental broadening because big crystal of the sample of our interest is not possible. According to this method, the instrumental broadening is about 0.1º.

The crystallite size of tetragonal ZrO_2 phase was calculated 4.7 nm after the subtraction of the instrumental peak broadening.

The sample calcined at 773 K for 5 h (WZ) is still a mixture of tetragonal ZrO_2 phase and randomly oriented mesoporous ZrO_2 phase (Fig. 4). The peak at low angle shifts to the left until the heat treatment at 873 K. This means that an opening of pores takes place. The peak intensities of tetragonal ZrO_2 phase for WZ are higher than those for WZ 650. Contrary, the intensity of the peak at 1.8º for WZ decreases relative to that of the peak at 2º for WZ 650. It indicates that after calcination, there is a simultaneous increase in the amount of the tetragonal ZrO_2 phase and decrease in the amount of the mesoporous phase. The tetragonal crystallite size is 4.9 nm for WZ. There is a small crystallite size difference between WZ 650 and WZ. It can be concluded that the presence of tungsten oxide and mesoporous phase stabilizes tetragonal ZrO_2 crystallites and retard the growth of ZrO_2 grains. This is consistent with the literature data [66-68].

Powder X-ray diffraction patterns of the heat treated samples (WZ600HT and WZ700HT) show that samples contain only crystalline tetragonal zirconia phase and the intensity of the peak at low angle belonging to mesoporous phase decreases considerably for WZ600HT and disappears completely for WZ700HT. It means that the mesoporous phase is not stable and pores collapse at high temperature. Furthermore the crystallite size of the tetragonal zirconia phase increases.

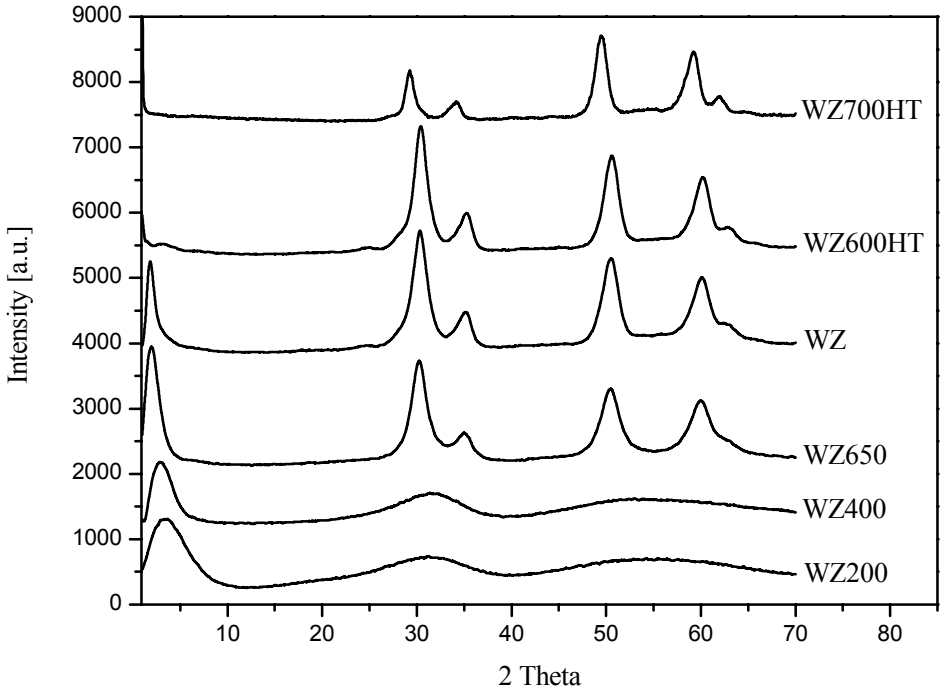

Figure 4. Effects of the heating at 473 K and at 673 K, carbonization at 923 K, calcination at 773 K and heat treatments at 873 K and at 973 K on the X-ray diffraction patterns during the preparation of the tungstated zirconia sample.

3. 1. 1. 2. Zirconia

The X-ray diffraction pattern of the heated sample at 673 K, denoted by Z 400, shows one broad peak at 5.1º and two broad features in the range of 2θ from 22 to 40º and from 40 to 70º (Fig. 5). The broad peaks show that the sample has a very low degree of crystallinity. There is a mesoporuous phase in the sample, which can be determined from the peak at low angle [64].

The diffractogram of the carbonized sample at 873 K, designated by Z 600, reveals that it consists of crystalline tetragonal zirconia phase and randomly distributed mesoporous phase.

The sample calcined at 773 K for 5 h, represented by Z, is a mixture of tetragonal and monoclinic ZrO_2 phases (Fig. 5). The peak at low angle shifts to the left after each heat treatment. It means that pore widening takes place. The peak intensity of mesoporous phase for Z decreases sharply. It can be concluded

that most of the mesoporous phase disappears and/or pores collapse at 773 K. The crystallite size of the tetragonal phase is 7.7 nm for Z.

The crystallographic phase compositions were calculated by using the Toraya et al. [69]. Then, the volume percentage of the tetragonal zirconia is 39%.

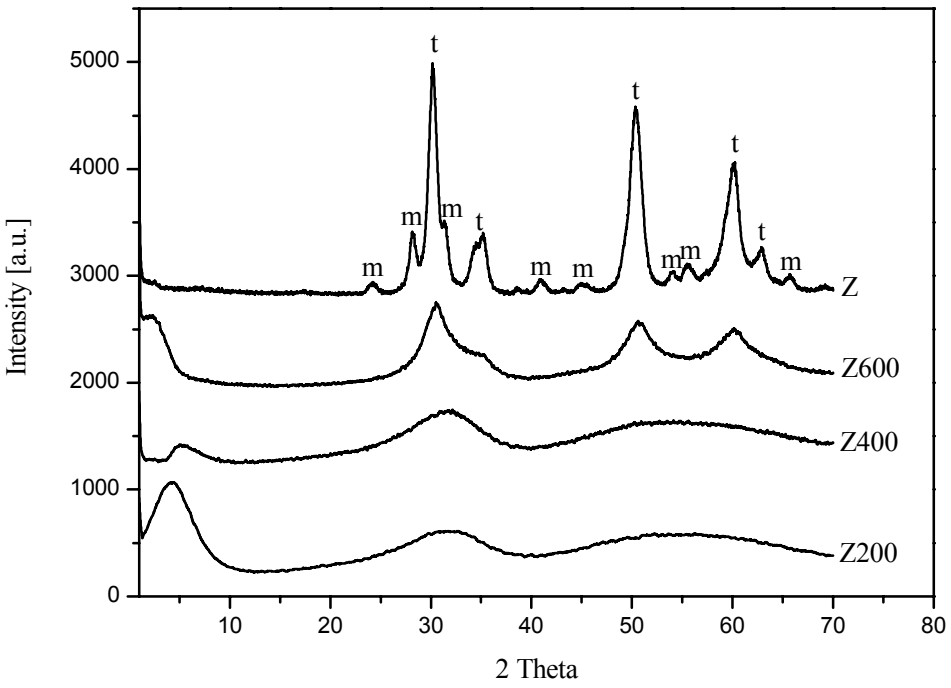

Figure 5. Effects of the heating at 473 K and at 673 K, carbonization at 873 K and calcination at 773 K on the X-ray diffraction patterns during the preparation of the pure zirconia sample (t: tetragonal, m: monoclinic).

3. 1. 1. 3. Palladium modified Tungstated zirconia

Diffractogram of Pd impregnated on tungstated zirconia shows that it contains the crystalline tetragonal zirconia phase and randomly distributed mesoporous phase. But phase transformation from tetragonal to monoclinic has started in the sample, which can be differentiated from the appearance of the small peaks in Fig. 6.

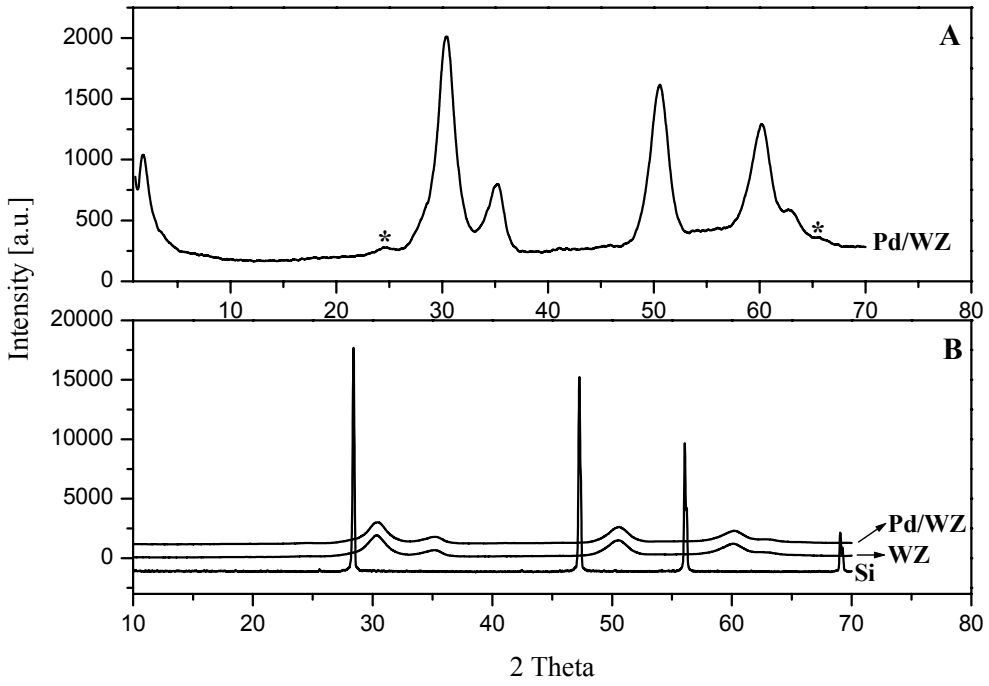

Figure 6. A: X-ray diffraction pattern after the preparation of Pd modified tungstated zirconia sample (* indicates the monoclinic phase). B: X-ray diffraction patterns of the sample for comparison.

3. 1. 2. Tungsten Density

Theoretically the atomic ratio of Zr to W (Zr:W) was chosen 8.25:1, corresponding to 18.6% of WO_3 by a mass content. This corresponds to nominal surface density of 2.8 WO_3/nm^2, which is 0.5 of the monolayer. The coverage is obtained by using the maximum packing density of planar WO_3 species equal to 0.21 g $WO_3/100m^2$ [42].

3. 1. 3. FT-IR Spectra of the Activated Samples

Fig. 7 shows FT-IR spectra of the activated Pd/WZ catalyst (spectrum c), WZ support (spectrum b) together with pure zirconia (spectrum a). The activated spectrum of the ZrO_2 in the OH-stretching region displays a pair of bands at 3770 and 3744 cm^{-1}, strong absorption at 3645 cm^{-1} and a broad band

between 3500 and 3000 cm^{-1}. According to the literature data [29,61,70], the band at 3770 cm^{-1} is attributed to terminal OH-groups due to the monoclinic phase. The band at 3744 cm^{-1} belongs to bibridged OH-groups and the band at 3645 cm^{-1} is assigned to tribridged OH groups from the monoclinic and tetragonal phases. The broad band is attributed to H-bonded tribridged hydroxyls. The band at 2342 cm^{-1} corresponds to adsorbed CO_2 [69]. Bolis et al. [71] reported that relatively stable CO_2 adsorbed on tetragonal zirconia resisting room temperature evacuation. The bands in the 1700 - 1100 cm^{-1} region are assigned to surface carbonates [70]. Most probably CO_2 appears as a product of the decomposition of the residual carbonates (produced from burning of the sample and adsorb on the surface when the temperature is lowered.

The spectrum of the tungstated zirconia sample (Fig. 7, spectrum b) in the OH-stretching region is characterized by the bands corresponding to bibridged terminal OH-groups (3744 cm^{-1}) [29] and tribridged terminal hydroxyls (3645 cm^{-1}) of the tetragonal zirconia. An intense band at 1009 cm^{-1} due to $\nu(W=O)$ and the respective overtone at 2009 cm^{-1} [72,73] are observed. These bands are typical of wolframyl species (W^{6+} =O) supported on zirconia [73]. The broad band in the 3600-3000 cm^{-1} region and band at 1602 cm^{-1} are due to adsorbed water, which requires prolonged activation in order to remove. The bands in the 1550 - 1100 cm^{-1} region are assigned to surface carbonates [29,70].

The spectrum of Pd/WZ catalyst is similar to that of WZ. The amount of adsorbed water is lower and no surface carbonates are observed.

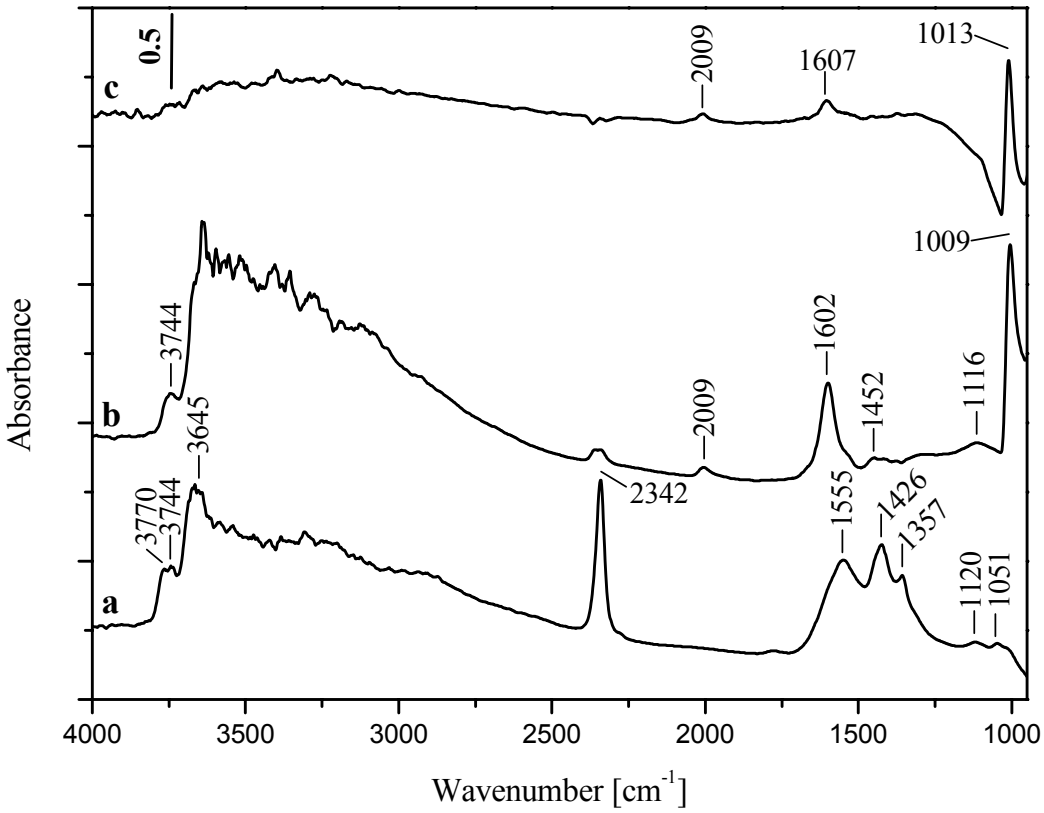

Figure 7. FT-IR spectra of the activated zirconia (a), WZ sample (b) and Pd/WZ catalyst (c). The spectra are taken at ambient temperature.

3. 2. NO and NO/O_2 Adsorption and Thermal Stability of the Adsorbed NO_x species

3. 2. 1. Adsorption of NO

3. 2. 1. 1. Adsorption of NO at Room Temperature on ZrO_2

Spectra of NO (1.34kPa) adsorbed at room temperature on the zirconia sample for a period of 20 min are shown in Fig. 8. The intense band at 1190 cm^{-1} (Fig. 8, spectrum b) is assigned to the ν(NO) stretching mode of anionic nitrosyl, NO^- [61]. These species can form by disproportionation NO on the surface O^{2-} sites:

$$3NO + O^{2-} \rightarrow NO_2 + 2NO^- \qquad (1)$$

The NO_2 produced can be adsorbed on the surface, leading to formation of NO_3^- and NO_2^- species (bands in the 1600-1000 cm^{-1} region) [61,62,74]. The presence of adsorbed NO_x species causes perturbation of the isolated OH groups at 3745 cm^{-1} and appearance of hydrogen-bonded hydroxyls. The weak band 1682 cm^{-1} is assigned to cis-HNO_2 [61].

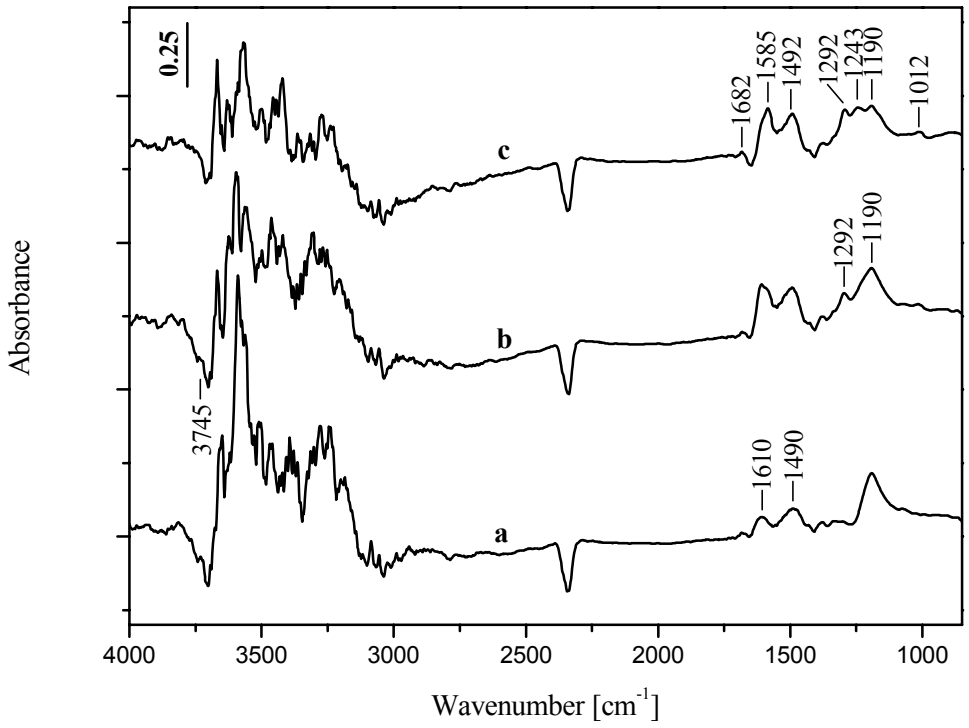

Figure 8. FTIR spectra of adsorbed NO (1.34 kPa) on pure zirconia sample at room temperature immediately (a), for 20 min (b), and after evacuation (c). The spectrum of the activated sample is used as a background reference.

3. 2. 1. 2. Adsorption of NO on WZ at Room Temperature

Spectra of NO (1.34 kPa) adsorbed at room temperature on the WZ sample are shown in the Fig. 9. The equilibrium between the gaseous NO and the adsorbed NO_x species is established after 10 min. The band at 1180 cm^{-1} is attributed to $\nu_{as}(NO_2)$ mode of bidentate nitrito species [62]. The pair of bands at 1455 and 1425 cm^{-1} are assigned to the $\nu_{as}(NO_2)$ modes of two types of

monodentate nitro species [62]. This assignment is consistent with the fact that they resist evacuation at room temperature (see Fig. 9, spectrum c). In general, the nitro species are more stable than the nitrito species. The $\nu_s(NO_2)$ modes of the nitro and nitrito species fall below 1100 cm^{-1} and cannot be detected. The fact that NO_2^- species are formed indicates that the adsorbed NO undergoes oxidation. Since Zr^{4+} ions are considered to be unreducible under these conditions, the following process, in which the surface hydroxyls at 3751 cm^{-1} and W^{6+} ions are involved, can be suggested:

$$2NO + W^{6+} + 2OH^- \rightarrow N_2O_3 + H_2O + W^{4+} \qquad (2)$$

Indeed, appearance of a negative band at 3751 cm^{-1} and the positive absorption in the 3500 – 3000 cm^{-1} support the participation of the Zr^{4+}–OH groups in this process leading to formation of adsorbed water molecules ($\delta(H_2O)$ at 1600 cm^{-1}). The bands at 2054 and ~ 1992 cm^{-1} together with the weak absorption at 1350 and 1311 cm^{-1} correspond to the ν(N=O) and $\nu_s(NO_2)$ modes of N_2O_3 adsorbed on two different sites [59,74]. The $\nu_{as}(NO_2)$ stretching vibration is overlapped by the water band at 1600 cm^{-1}. It can be proposed that N_2O_3 undergoes self-ionization according to the reaction:

$$N_2O_3 \Leftrightarrow NO^+ + NO_2^- \qquad (3)$$

The NO^+ species are identified by the absorption band at 2130 cm^{-1} due to the ν(NO) mode [59,61]. Most probably the NO_2^- species obtained in this process are the bidentate nitrites at 1180 cm^{-1}. They disappear together with the adsorbed N_2O_3 and NO^+, which confirms the occurrence of the equilibrium (3). The bands at 2284 and 2246 cm^{-1} are assigned to the ν(NN) modes of N_2O adsorbed on two different sites [59,74]. The ν(NO) stretching vibration is at 1224 cm^{-1}. The weak band at 2446 cm^{-1} is due to the first overtone of the ν(NO) fundamental band of N_2O. Since no Zr^{4+}–NO bands are observed on the pure zirconia (see page 23, Fig. 8), the absorption at 1915 cm^{-1} is attributed to Zr(IV) species, of with wolframyl groups are in their vicinity.

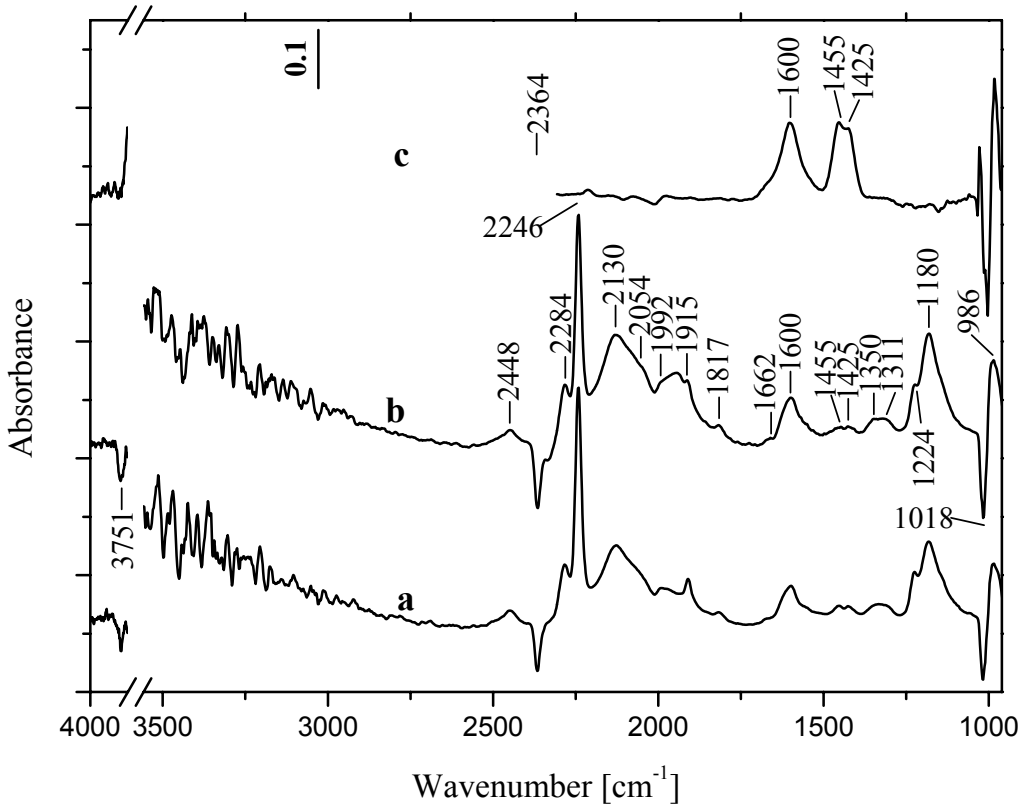

Figure 9. FTIR spectra of adsorbed NO (1.34 kPa) on the WZ support at room temperature immediately (a), for 10 min (b), and after evacuation at room temperature for 15 min. The spectrum of the activated sample is used as a background reference.

The weak band at 1662 cm^{-1} is assigned to the ν(N=O) modes of adsorbed cis-HNO_2 molecules [61], which are produced by interaction of the NO_2^- species with the adsorbed water:

$$NO_2^- + H_2O \leftrightarrow HNO_2 + OH^- \qquad (4)$$

An assignment of the IR bands observed upon NO adsorption on the WZ support is summarized in Table 5.

Table 5. Assignments of the FT-IR bands observed upon NO adsorption on the WZ support.

NO_x species	**Band Position (cm^{-1})**	**Mode**
NO^+	2130	ν(NO)
H_2O	1600 3751	δ(H_2O) ν(OH)
cis-HNO_2	1662	ν(N=O)
Bidentate nitrito, NO_2^-	1180	$\nu_{as}(NO_2)$
Monodentate nitro, NO_2^- (two types)	1455 1425	$\nu_{as}(NO_2)$
N_2O_3 (two different sites)	2054, 1992 1350, 1311 1600	ν(N=O) $\nu_s(NO_2)$ $\nu_{as}(NO_2)$
N_2O (two different sites)	2284, 2246 1224 2446	ν(NN) ν(NO) 2ν(NO)
Zr^{4+}–NO	1915	ν(NO)

3. 2. 1. 3. Adsorption of NO on Pd/WZ at Room Temperature

Spectra of adsorbed NO (1.34 kPa) on the Pd/WZ catalyst at room temperature are similar to those observed for the tungstated zirconia. Following differences should be noticed:

1. There are no Zr^{4+}–NO nitrosyls.
2. The bands at 1863 and 1810 cm^{-1} are due to NO adsorbed on two different Pd(II) sites [75,76].
3. The adsorbed N_2O_3 (1935 and 1558 cm^{-1}) and the nitrito species at 1166 cm^{-1} resist the evacuation. Since the surface OH groups are not perturbed, the following process leading to N_2O_3 formation can be proposed:

$$2NO + WO^{4+} \rightarrow N_2O_3 + W^{4+} \qquad (5)$$

Involvement of the wolframyl species is confirmed by the appearance of a negative band at 1012 cm^{-1}.

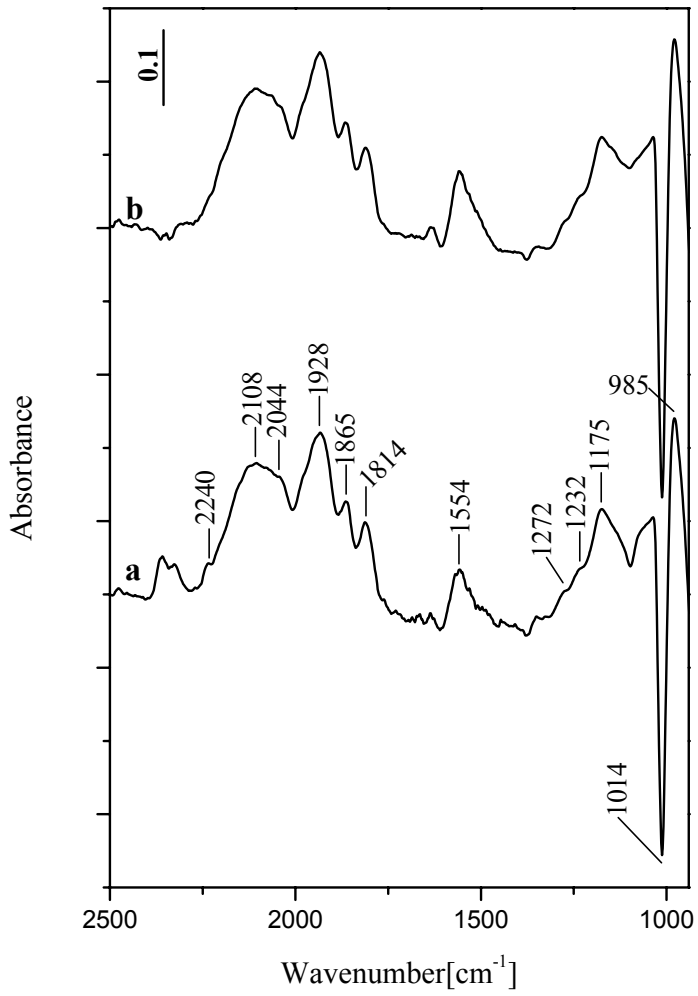

Figure 10. FT-IR spectra of adsorbed NO (1.34 kPa) on the Pd/WZ catalyst at room temperature for 40 min (a) and after evacuation (b). The spectrum of the activated sample is used as a background reference and the gas phase spectra are subtracted.

3. 2. 1. 4. High Temperature Adsorption of NO on the Pd/WZ Catalyst

Figure 11 shows the spectrum of the Pd/WZ catalyst taken after adsorption of NO (1.33 kPa) for 15 min (spectrum a) at room temperature, followed by heating the closed IR cell for 15 min at 623 K (spectrum b). The latter treatment causes all of the NO_x species observed at room temperature to disappear. Two new bands at 1837 and 1790 cm^{-1} (shoulder) and weak band at 1610 cm^{-1} are detected. The gas phase spectrum recorded at 623 K (not shown)

contains NO_2 in addition to NO. Some amount of N_2O is also detected, which was formed already at room temperature. Based on this, the band at 1610 cm^{-1} in spectrum b (Fig. 11) is attributed to adsorbed NO_2. This experimental fact shows that oxidation of NO to NO_2 has occurred. In this process the Pd^{2+} sites are involved because the W^{6+}=O species are almost completely restored, whereas strong perturbation in the region of the Pd^{2+}–NO nitrosyls is observed. The weak bands at 1863 and 1816 cm^{-1} corresponding to two types of Pd^{2+}–NO nitrosyls have disappeared and considerably stronger bands at 1837 and at about 1790 cm^{-1} (shoulder) are observed instead. These two bands are assigned to two different Pd^{+}–NO linear species, which correspond to the Pd^{2+}–NO nitrosyls observed at room temperature. The Pd^{+}–NO nitrosyls display high thermal stability and do not disappear upon evacuation at 623 K (Fig. 11, spectrum c). Increasing the temperature of the closed IR cell to 773 K (Fig. 11, spectra d and e) leads first to removal of the adsorbed NO_2 and then to loss of NO adsorbed on the Pd^{+} sites. Cooling back to room temperature (Fig. 11, spectra from f to h) causes reappearance of Pd^{+}–NO bands with reduced intensities, which indicates further oxidation of the adsorbed NO. The intensity of the band due to the adsorbed NO_2 (1610 cm^{-1}) increases with lowering the temperature, reaching maximum at 523 K. This band disappears at room temperature due to conversion of the adsorbed NO_2 to surface nitrate and nitro species (1610, 1587, 1457 and 1360 cm^{-1}).

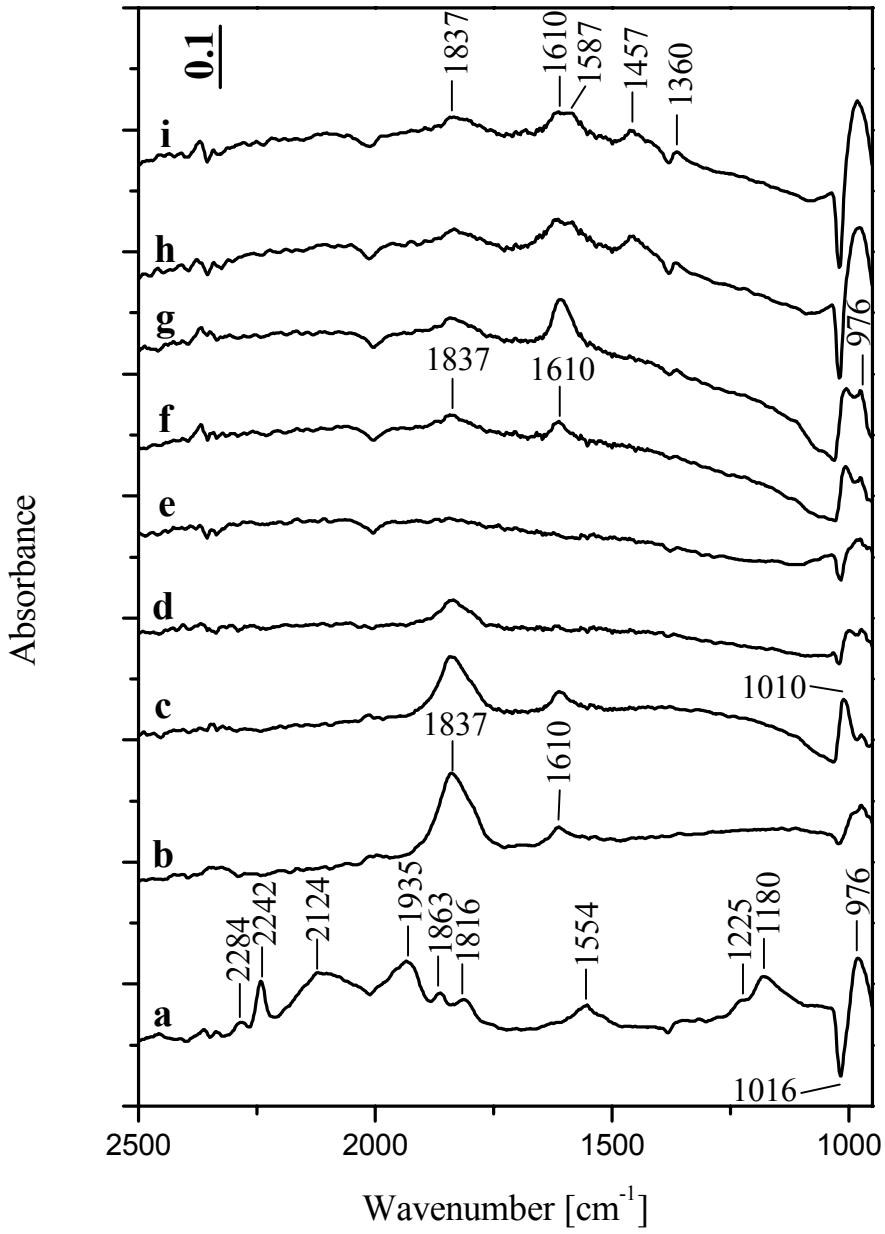

Figure 11. FT-IR spectra of the Pd/WZ sample taken after adsorption of NO (1.33 kPa) at room temperature for 15 min (a), after heating of the closed IR cell for 15 min at 623 K (b), and subsequent evacuation for 15 min at 623 K (c) then continuing heating the closed IR cell for 15 min at 723 K (d), at 773 K (e). Afterwards the closed IR cell was cooled to 623 K (f) to 523 K (g) and to RT (h). The spectrum of the activated sample is used as a background reference and the gas phase spectra are subtracted.

3. 2. 2. Coadsorption of NO/O_2 and Thermal Stability of NO_x produced

3. 2. 2. 1. On the ZrO_2 Sample

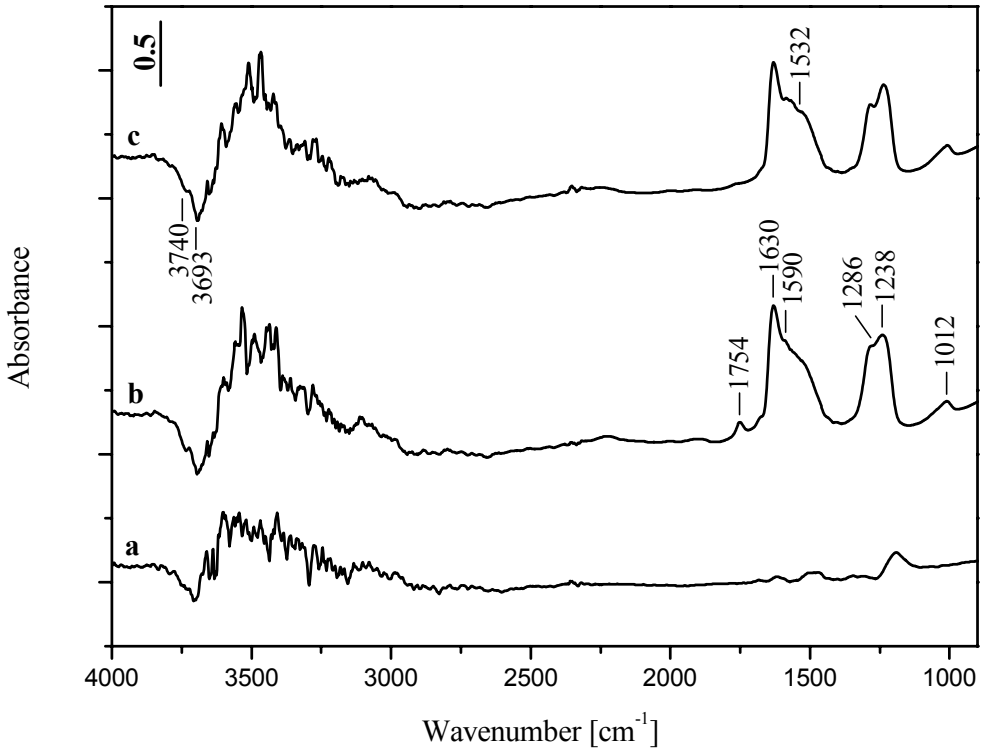

Figure 12. FT-IR spectra of NO (1.34 kPa) adsorbed on the zirconia support at room temperature for 10 min (a), after subsequent introduction of O_2 (2.66 kPa) for 35 min (b), and after evacuation for 15 min at ambient temperature (c). The spectrum of the activated sample is used as a background reference.

Fig. 12 shows the spectra of the zirconia support obtained after the adsorption of 1.34 kPa of NO for 10 min (Fig. 12, spectrum a). Subsequent addition of 2.66 kPa of O_2 to the IR cell for 35 min (Fig. 12, spectrum b) causes formation of NO_2 (the color of the gas phase has changed to brown) and disappearance of the band at 1190 cm^{-1} corresponding to the ionic nitrosyl. The band at 1754 cm^{-1}, which disappears after the evacuation at room temperature, is characteristic of adsorbed N_2O_4 [59]. The strong bands between 1650 and 1200 cm^{-1} correspond to various surface nitrates. The increase in the intensities of the

negative bands at 3740 and 3693 cm^{-1}, which is accompanied by appearance of positive absorption in the region of the H-bonded OH groups, suggests that the surface nitrates are formed by disproportionation of NO_2 with the involvement of the isolated surface hydroxyls [77,78]:

$$2OH^- + 3NO_2 \rightarrow 2NO_3^- + NO + H_2O \qquad (6)$$

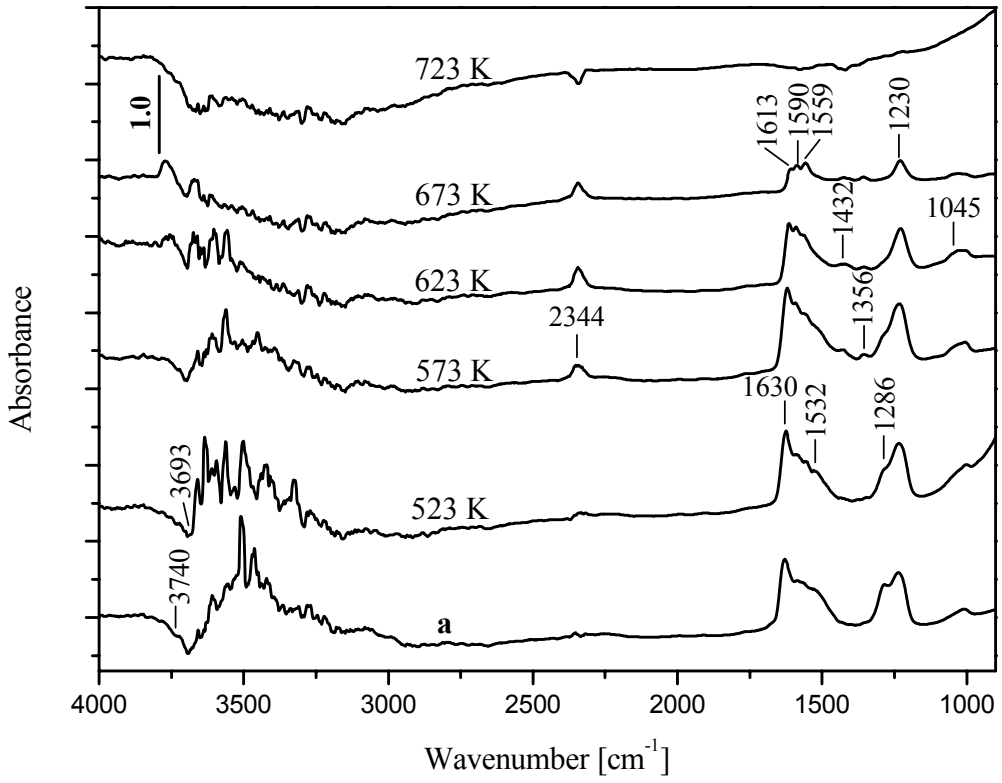

Figure 13. FT-IR spectra obtained after adsorption of NO/O_2 at RT followed by evacuation for 10 min (a), after heating the zirconia containing adsorbed NO_x species for 15 min in vacuum. The spectra are recorded after cooling of the IR cell to the room temperature. The spectrum of the activated sample is used as a background reference.

The nitrate species resist room-temperature evacuation (Fig. 12, spectrum c). However, heating the NO_x- precovered sample under vacuum in the 523 – 573 K temperature range (Fig. 13, spectra b and c) causes disappearance mainly of the monodentate nitrates at 1532 and 1286 cm^{-1} [59]. The bidentate

(1630, 1590 and 1233 cm^{-1}) nitrates display higher thermal stability and disappear from the spectrum after dynamic evacuation at 723 K [59,62].

The assignment of the IR bands observed upon NO/O_2 coadsorption on the zirconia sample is summarized in Table 6.

Table 6. Assignments of the FT-IR bands observed upon NO/O_2 coadsorption on the zirconia sample.

NO_x species	**Band Position (cm^{-1})**	**Mode**
Monodentate NO_3^-	1532 1286	$\nu_{as}(NO_2)$ $\nu_s(NO_2)$
Bidentate NO_3^-	1630-1613,1590,1559 1230	$\nu(N=O)$ $\nu_{as}(NO_2)$
N_2O_4	1754	$\nu(N=O)$

3. 2. 2. 2. On the WZ Support

Figure 14 shows the spectra of the WZ support obtained after the adsorption of 1.34 kPa of NO for 10 min (Fig. 14A, spectrum a), followed by the addition of 2.66 kPa of O_2 to the IR cell for 30 min (Fig. 14A, spectrum b). Compared to the pure zirconia, the amount of the adsorbed species observed in the presence of the gas phase is considerably larger. The weakly adsorbed species, which disappear after evacuation at room temperature (Fig. 14B), are identified as follows (see Table 7 for the assignment of the bands): N_2O_3 adsorbed on two different sites (1945, 1885, 1582, 1514, 1288 and 1274 cm^{-1}), N_2O_4 (1745 and 1288 cm^{-1}) and NO_2 (1618 cm^{-1}) [59,78]. The strong band at 2185 cm^{-1}, which decreases in intensity after the evacuation, is typical of NO^+ species. Formation of large amounts of oxides of nitrogen with oxidation numbers +3 and +4, which is not observed in the case of NO/O_2 adsorption on pure zirconia, suggests that in the oxidation of NO not only O_2 but also the wolframyl, W^{6+}=O, species are involved. This is confirmed by the appearance of a negative band at 1012 cm^{-1}

(shifted to 984 cm^{-1}) due to perturbed wolframyl groups. The following processes can be proposed:

$$NO + WO^{4+} \rightarrow NO_2 + W^{4+} \quad (7)$$

$$NO + NO_2 \rightarrow N_2O_3 \quad (8)$$

$$2NO_2 \rightarrow N_2O_4 \quad (9)$$

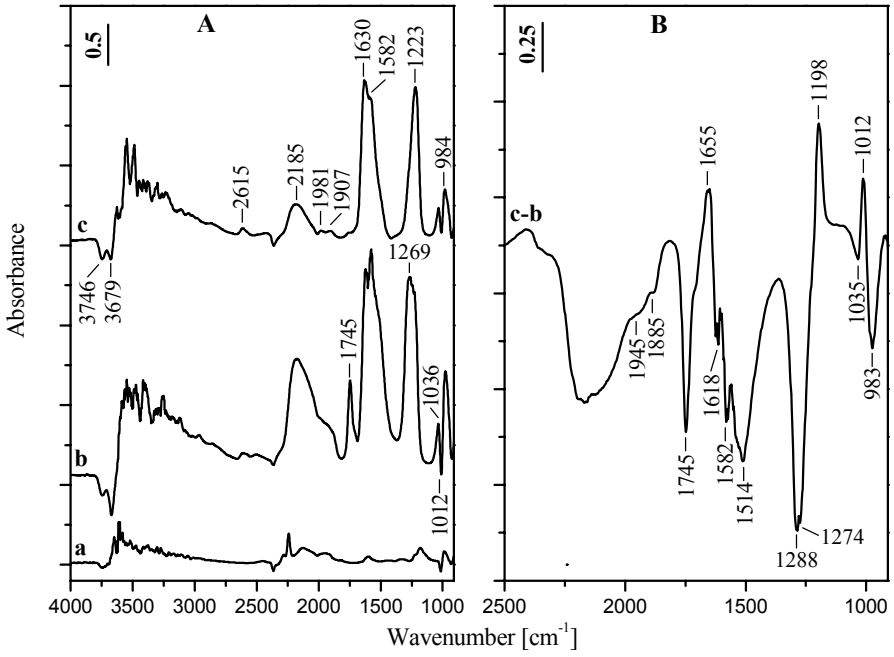

Figure 14. (A) FT-IR spectra of NO (1.34 kPa) adsorbed on the WZ support at room temperature for 10 min (a), after subsequent introduction of O_2 (2.66 kPa) for 30 min (b), and after evacuation for 10 min at ambient temperature(c). The spectrum of the activated sample is used as a background reference. (B) FT-IR subtraction spectra of the WZ sample obtained from the spectra drawn in A.

As in the case of pure zirconia, the bands at 1630, 1582 and 1223 cm^{-1} resisting the evacuation correspond to bidentate nitrates. They can form by both disproportionation (reaction 6) and self-ionization of NO_2/N_2O_4 [61]:

$$N_2O_4 \text{ (or } 2NO_2) \leftrightarrow NO^+ + NO_3^- \quad (6)$$

The weak bands at 2615, 1981, and 1907 cm^{-1} (Fig. 14A, spectrum c) correspond to combination modes of the fundamental nitrate bands.

Table 7. Assignments of the FT-IR bands observed upon NO/O_2 coadsorption on the WZ support.

Species	**Band, cm^{-1}**	**Mode**
NO^+	2185	$\nu(NO)$
N_2O_4	1745, 1288	$\nu_{as}(NO_2)$ $\nu_s(NO_2)$
N_2O_3	1945, 1885 1582,1514 1288,1274	$\nu(N=O)$ $\nu_{as}(NO_2)$ $\nu_s(NO_2)$
NO_2	1618	$\nu_{as}(NO_2)$
Monodentate NO_3^-	1514 1274 1035	$\nu_{as}(NO_2)$ $\nu_s(NO_2)$ $\nu(N=O)$
Bidentate NO_3^-	1630, 1582 1223 1755 2614	$\nu(N=O)$ $\nu_{as}(NO_2)$ $\nu_s(NO_2) + \delta(ONO)$ $\nu(N=O) + \nu_s(NO_2)$

The thermal stability of the adsorbed NO_3^- species is lower than that on pure zirconia. They disappear after the evacuation at 673 K (Fig. 15). The negative absorption in the 3600 – 3000 cm^{-1} region and the band at 1600 cm^{-1} observed in the spectra d and e (Fig. 15) are due to desorbed water molecules initially present in the activated sample. The weak negative bands at 1455 and 1425 cm^{-1} indicate that there is a loss in the carbonate species present as

contaminations on the surface of the WZ sample. The adsorbed NO_x species facilitate desorption of adsorbed water and carbonate impurities, which were difficult to remove during the activation of the sample.

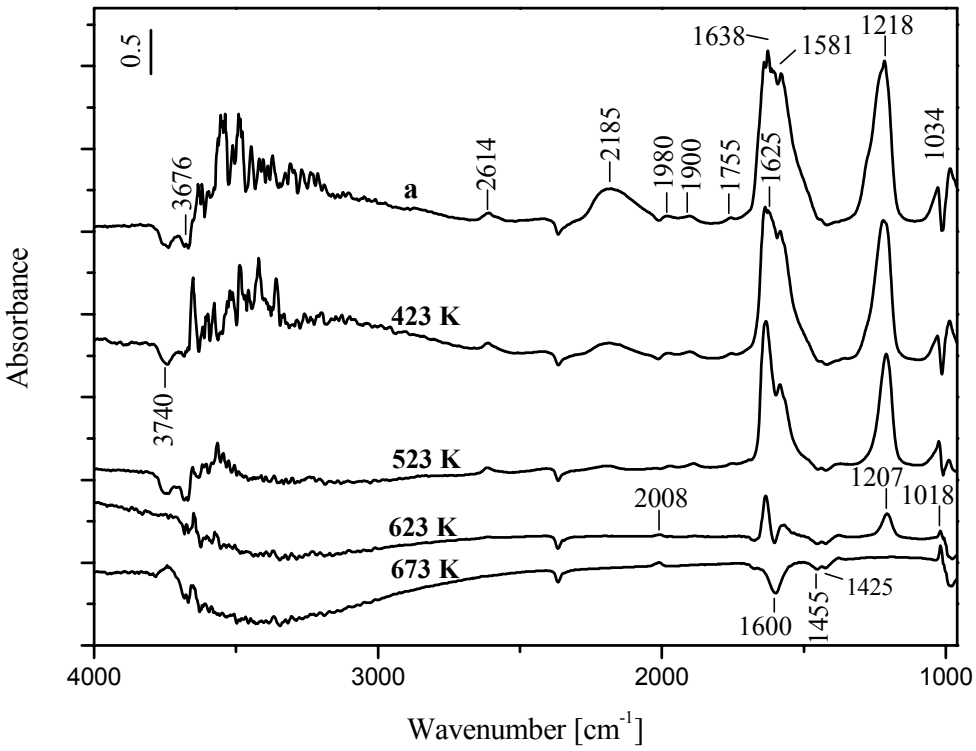

Figure 15. FT-IR spectra obtained after adsorption of NO/O_2 at RT followed by evacuation for 10 min (a), after heating the WZ sample containing adsorbed NO_x species for 15 min in vacuum. The spectra are recorded after cooling of the IR cell to the room temperature. The spectrum of the activated sample is used as a background reference.

3. 2. 2. 3. On the Pd/WZ Catalyst

Figure 16 shows the spectra of the Pd/WZ sample recorded after the adsorption of 1.34 kPa of NO for 25 min (Fig. 16A, spectrum a), followed by the addition of 2.66 kPa of O_2 to the IR cell for 30 min (Fig. 16A, spectrum b). The spectrum of adsorbed NO/O_2 shows new bands in the region between 1800 and 1200 cm^{-1} (subtraction spectrum b-a in Fig. 16B). During the NO/O_2 adsorption no change in the ν(OH) stretching region is observed in the spectra. The gas phase

spectrum (corresponding to the conditions of spectrum b) shows the formation of N_2O_3 and N_2O_4/NO_2 [59,74,78]. These gases adsorb (see also the subtraction spectrum b-a in Fig. 16B) on the surface producing bands at 1910 and 1876 cm^{-1} (N_2O_3) and 1750 and 1712 cm^{-1} (N_2O_4 adsorbed on two different sites). The ν(N=O) mode of the N_2O_3 overlaps the Pd^{2+}–NO band at 1876 cm^{-1} [75,76]. As in the case of the WZ sample (see Section 3.2.2.2) the absorption at 1976 cm^{-1} corresponds to the ν(NO) stretching vibration in the complex $ON–Zr^{4+}–ONO_2^-$ [61]. The broad band with maximum at about 2160 cm^{-1} reveals the presence of NO^+ ions. These species can be produced by self-ionization of the adsorbed N_2O_4 with the participation of Lewis acid-base pairs according to reaction (6).

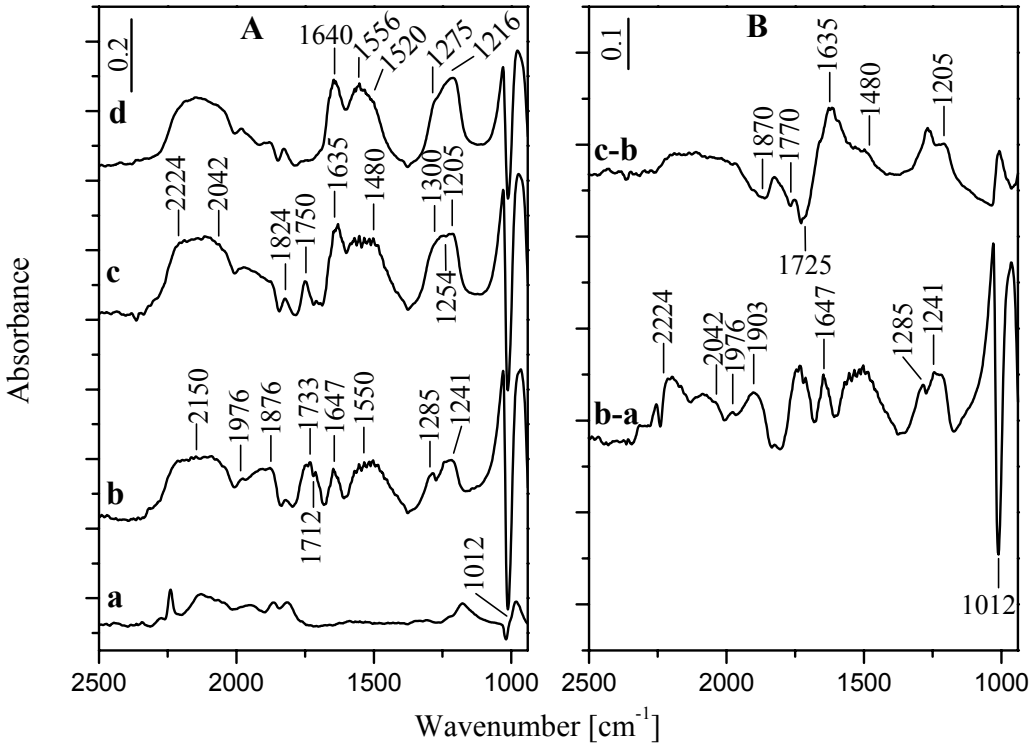

Figure 16. (A) FT-IR spectra of NO (1.34 kPa) adsorbed on the Pd/WZ catalyst at room temperature for 25 min (a), after subsequent introduction of O_2 (2.66 kPa) for 30 min (b), after evacuation for 10 min (c) and for 30 min (d) at ambient temperature. The spectrum of the activated sample is used as a background reference and the gas phase spectra are subtracted. (B) FT-IR subtraction spectra of the Pd/WZ sample obtained from the spectra drawn in A.

The nitrate species are identified by the band at 1647 cm^{-1} due to the ν(N=O) stretching vibration (bridging coordination mode) [62]. The characteristic stretching vibrations of the bidentate and monodentate nitrates species fall in the 1600 – 1400 and 1300 –1200 cm^{-1} regions and cannot be resolved. The negative band at 1012 cm^{-1} indicates strong perturbation of the W^{6+}=O species. The band at 1020 cm^{-1}, which is offset by the negative band at 1012 cm^{-1}, is due to the $\nu_s(NO_2)$ modes of the nitrate species. The subtraction spectrum b-a in Fig. 16 shows loss in the intensities of the Pd^{2+}–NO bands at 1876 and 1824 cm^{-1}, which most probably is due to replacement of the adsorbed NO by the nitrate species. The evacuation for 10 min at room temperature (Fig. 16A,spectrum c and Fig. 16B, spectrum c-b) causes removal of N_2O_3 (negative band at 1870cm^{-1}) and decrease in the intensity of the bands associated with adsorbed N_2O_4 (negative bands at 1750 and 1725 cm^{-1}). This is accompanied by increase in the intensities of the bands due to the charged species (NO^+ and NO_3^-) indicating that the evacuation favors the self-ionization of the N_2O_4. Extending the evacuation to 30 min (Fig. 16, spectrum d) causes almost complete removal of the adsorbed N_2O_4 and decrease in the intensity of the broad band due to NO^+ ions.

Upon evacuation for 10 min in the 383 – 623 K temperature range the broad absorption bands in the nitrate region loose intensities (Fig. 17). By using the subtraction spectra (not shown) it is found that the adsorbed N_2O_4 and the monodentate nitrates characterized by the bands at 1469 and 1295 cm^{-1} desorb first from the surface. Increasing the temperature to 523 K causes removal of the monodentate nitrates at 1535 and ~ 1254 cm^{-1}. The species characterized by the broad absorption between 1650 and 1500 cm^{-1} with a concomitant band at 1205 cm^{-1} display the highest thermal stability. They are attributed to bidentate nitrates species [59]. The corresponding absorption bands are observed with reduced intensities at 623 K and disappear upon the evacuation at 673 K. The thermal stability of the surface nitrates formed upon NO/O_2 adsorption at room temperature on the WZ and Pd/WZ samples is comparable.

The assignment of the FT-IR bands is shown in Table 8.

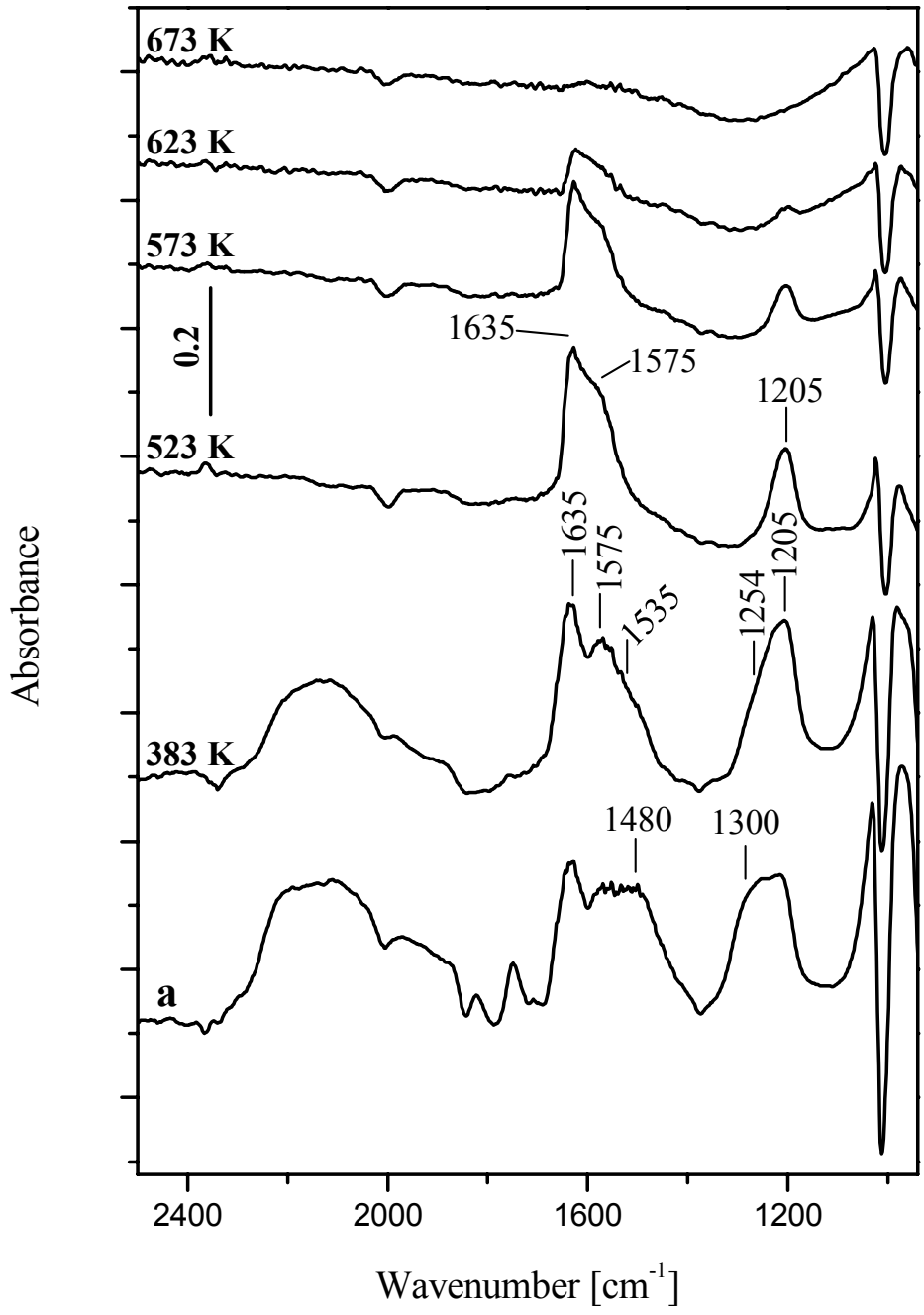

Figure 17. FT-IR spectra obtained after adsorption of NO/O_2 at RT followed by evacuation for 10 min (a), after heating the Pd/WZ sample containing adsorbed NO_x species for 10 min in vacuum. The spectrum of the activated sample is used as a background reference and the gas phase spectra are subtracted.

Table 8. Assignments of the FT-IR bands observed upon NO/O_2 coadsorption on the Pd/WZ catalyst.

Species	**Band, cm^{-1}**	**Mode**
NO^+	2160	$\nu(NO)$
$Pd^{2+} - NO$	1876, 1824	$\nu(NO)$
$ON - Zr^{4+} - NO_3^-$	1976	$\nu(NO)$
N_2O_4	1750, 1712 1285	$\nu_{as}(NO_2)$ $\nu_s(NO_2)$
N_2O_3	1910, 1876 1469 1295	$\nu(N=O)$ $\nu_{as}(NO_2)$ $\nu_s(NO_2)$
Monodentate NO_3^- (two types)	1469, 1535 1295, 1254	$\nu_{as}(NO_2)$ $\nu_s(NO_2)$
Bidentate NO_3^-	1650, 1500 1205 1020	$\nu(N=O)$ $\nu_{as}(NO_2)$ $\nu_s(NO_2)$

3. 2. 3. Summary of the Results on NO and NO/O_2 Adsorption on the Samples Studied

Adsorption of NO reveals the presence of coordinatively unsaturated Zr^{4+} ions on the tungstated zirconia. No such sites are observed on Pd/WZ catalyst.

The surface NO_x species observed during the room temperature adsorption of NO on WZ and Pd/WZ samples are produced by the involvement of the W^{6+}=O groups. The Pd(II) sites interact with NO upon heating at 623 K giving rise to adsorbed NO_2..

It is also observed that the stabilities of nitrito species and N_2O_3 are different on WZ and Pd/WZ samples. Even though adsorbed N_2O_3 and nitrito species on the WZ sample leave easily the surface upon evacuation at room temperature, those species on the Pd/WZ catalyst resist desorption upon evacuation. So the presence of Pd^{2+} changes the behavior of the species observed commonly on both samples.

Coadsorption of NO and O_2 at room temperature results in formation of various surface nitrates and gaseous species; e.g. NO_2, N_2O_4, N_2O_3. Oxidation of NO is due to O_2 and the wolframyl groups present on the samples. Nitrates and nitrosonium ions are observed on the WZ and Pd/WZ because of the self-ionization of N_2O_4. Evacuation in the 383-623 K temperature range shows that the surface nitrates have similar thermal stabilities for both samples. This and the lower surface concentration of the nitrate species show that in the case of the Pd/WZ catalyst they are coordinated to the support.

3. 3. Reactivity of the Adsorbed Coadsorption of NO/O_2 and Thermal Stability of NO_x produced

In order to evaluate the ability of the catalyst containing preadsorbed NO_x species for methane activation, the following experiments were performed:

(i) "Blank NO_x" experiment involves the formation of NO_x adsorbed species by NO/O_2 coadsorption, followed by evacuation at room temperature and heating the closed IR cell containing the NO_x-precovered catalyst at 723 K.

(ii) "Blank CH_4" experiment, which consists of interaction of the activated catalyst with methane at elevated temperatures.

(iii) "NO_x - CH_4" experiment involves the interaction of methane with the catalyst containing preadsorbed NO_x species at various temperatures.

3. 3. 1. "Blank NO_x" Experiment

3. 3. 1. 1. With The WZ Support

Heating the closed IR cell for 20 min at 723 K (Fig. 18, spectrum b) causes complete removal of the adsorbed NO_x species. After cooling to room temperature (spectrum c) bands due to readsorbed NO^+ ions (2140 cm^{-1}) and bidentate nitrates (1610 and 1187 cm^{-1}) are detected. The weak bands at 1457 and 1418 cm^{-1} indicate the presence of NO_2^- (monodentate nitrito or bridged nitro) species.

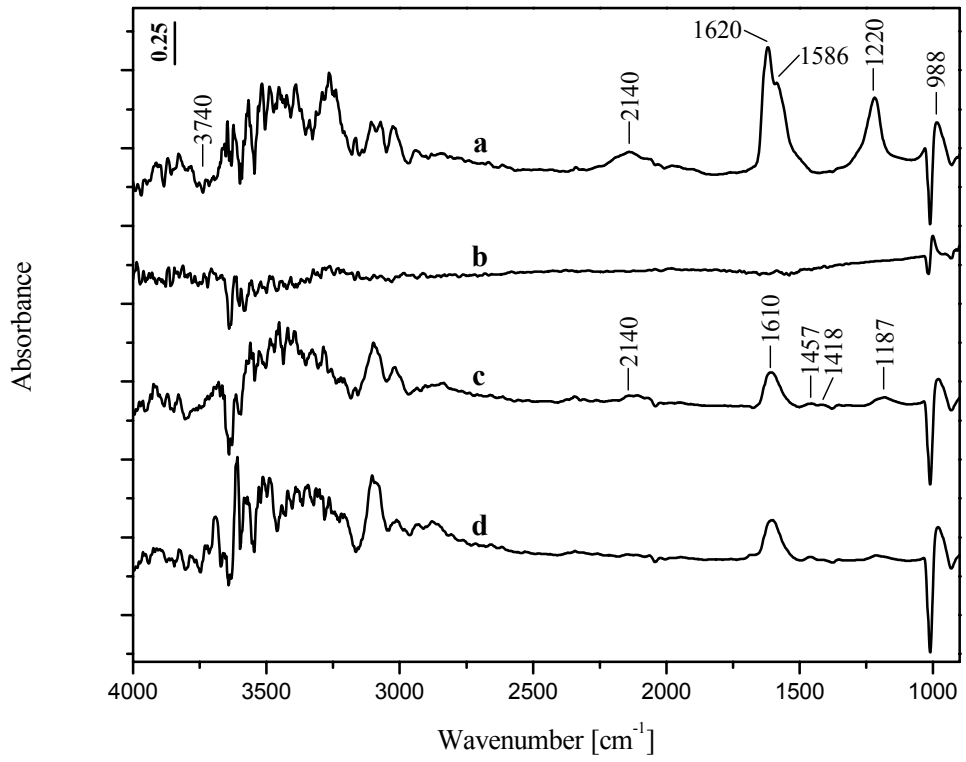

Figure 18. FT-IR spectra of the WZ support taken after adsorption of NO/O_2 mixture (1.33 kPa : 2.66 kPa, $NO:O_2$ = 1:2) at ambient temperature followed by evacuation down to $3x10^{-3}$ Torr (a), after heating of the closed IR cell for 20 min at 723 K (b), then cooling of it to RT (c), and then evacuation of the gas phase at RT (d). The spectrum of the activated sample is used as a background reference.

This experimental fact shows that decomposition of the surface nitrates has occurred. However, due to the low partial pressures of the decomposition products (NO_2, NO and O_2), they were not detected in the gas phase spectrum. This could be the reason that the adsorbed NO_x species are not completely restored. Another possible explanation is that some of the surface nitrates undergo decomposition to N_2 and O_2. However, in order to confirm this assumption, further experiments are needed.

3. 3. 1. 2. With The Pd/WZ Catalyst

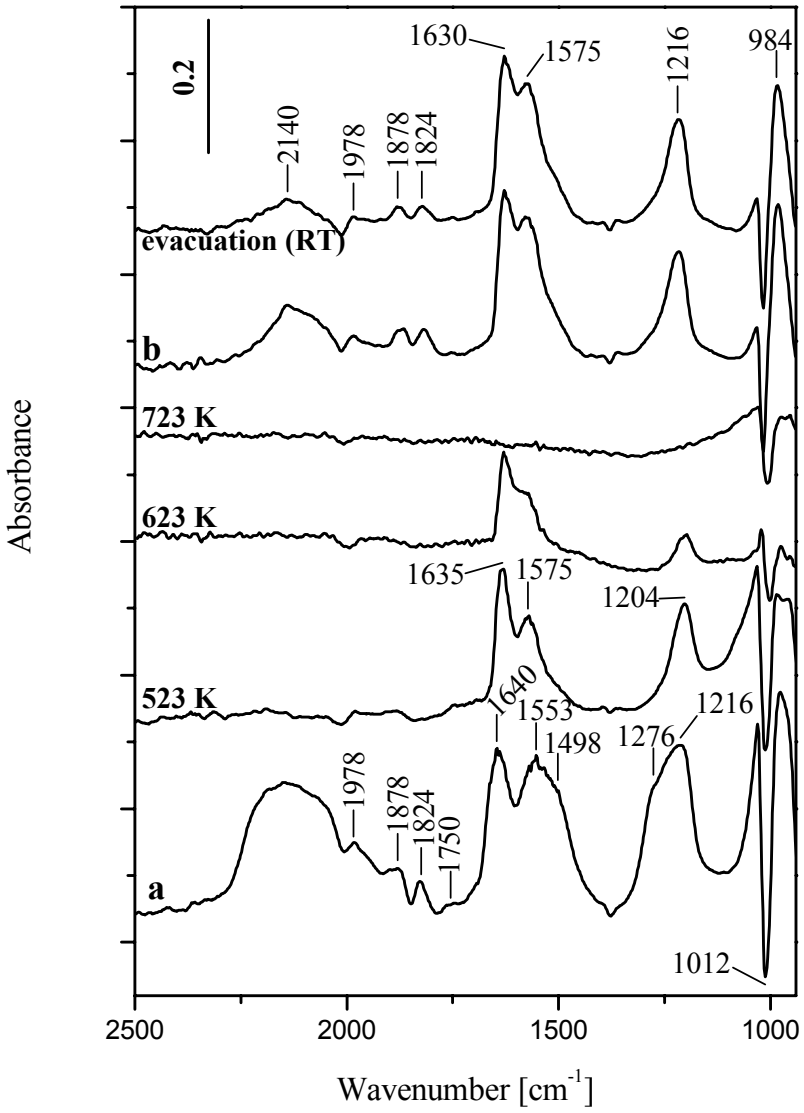

Figure 19. FT-IR spectra of the Pd/WZ sample taken after adsorption of NO/O_2 mixture (1.33 kPa : 2.66 kPa, $NO:O_2$ = 1:2) at room temperature followed by evacuation for 30 min (a), after heating of the closed IR cell for 15 min, then cooling to RT (b). The spectrum of the activated sample is used as a background reference and the gas phase spectra are subtracted.

The preadsorbed NO_x species are created on the surface of the Pd/WZ catalyst by exposing 1.33 kPa of NO and 2.66 kPa of O_2 ($NO:O_2$ = 1:2) for 30 min followed by evacuation for 30 min at room temperature (Fig. 19, spectrum a). Heating the closed IR cell for 15 min at 523 K leads to disappearance of the NO^+

species (2140 cm^{-1}), nitrato-nitrosyl complex (1978 cm^{-1}), Pd^{2+} – NO nitrosyls (1878 and 1824 cm^{-1}) and monodentate nitrates (1498, 1276). Complete removal of the adsorbed NO_x species occurs under heating the closed IR cell at 723 K (Fig. 19, spectrum at 723 K). The increase in the temperature causes decrease in the intensity of the negative band at 1010 cm^{-1} due to restoration of perturbed W^{6+}=O groups. However, the restored wolframyl species differ from the original ones, which is evident by the blue shift of the ν(W=O) band from 1009 to 1023 cm^{-1} (Fig. 19, spectrum at 723 K). Moreover, cooling the IR cell to room temperature (Fig. 19, spectrum b) results in reappearance of the NO^+ ions (2140 cm^{-1}), Pd^{2+}–NO nitrosyls (1878 and 1824 cm^{-1}) and bidentate nitrates (bands with maxima at 1630, 1575 and 1216 cm^{-1}). The amount of the perturbed W^{6+}=O species increases again as a result of the readsorption of the gaseous phase.

3. 3. 2. "Blank CH_4" Experiment

3. 3. 2. 1. With The WZ Support

Results of heating the activated WZ support under constant pressure of methane (8 kPa) in the closed IR cell in the temperature range 523 – 723 K are shown in Fig. 20. The oxidation of CH_4 starts already at 523 K (Fig. 20, spectrum a), which is evident by appearance of weak bands in the carbonate-carboxylate region [70] at 1660, 1608 and about 1520 cm^{-1}. Increasing the temperature to 723 K the corresponding adsorption forms disappear from the spectra. The spectrum obtained after cooling to room temperature contains strong band at 2362 cm^{-1} typical of adsorbed CO_2 [70]. In the low-frequency region the band at 1606 cm^{-1} reveals the formation of bidentate carbonates, whereas the pair of bands at 1460 and 1429 cm^{-1} can be assigned to two types of monodentate carbonates [70]. The weak bands at 1680 and 1230 cm^{-1} are typical of hydrogencarbonates [70]. All of the bands except that of CO_2 resist the room-temperature evacuation, which is in agreement with their assignments. The data show that the WZ sample is able to catalyze the complete oxidation of the CH_4. Taking into account the fact that

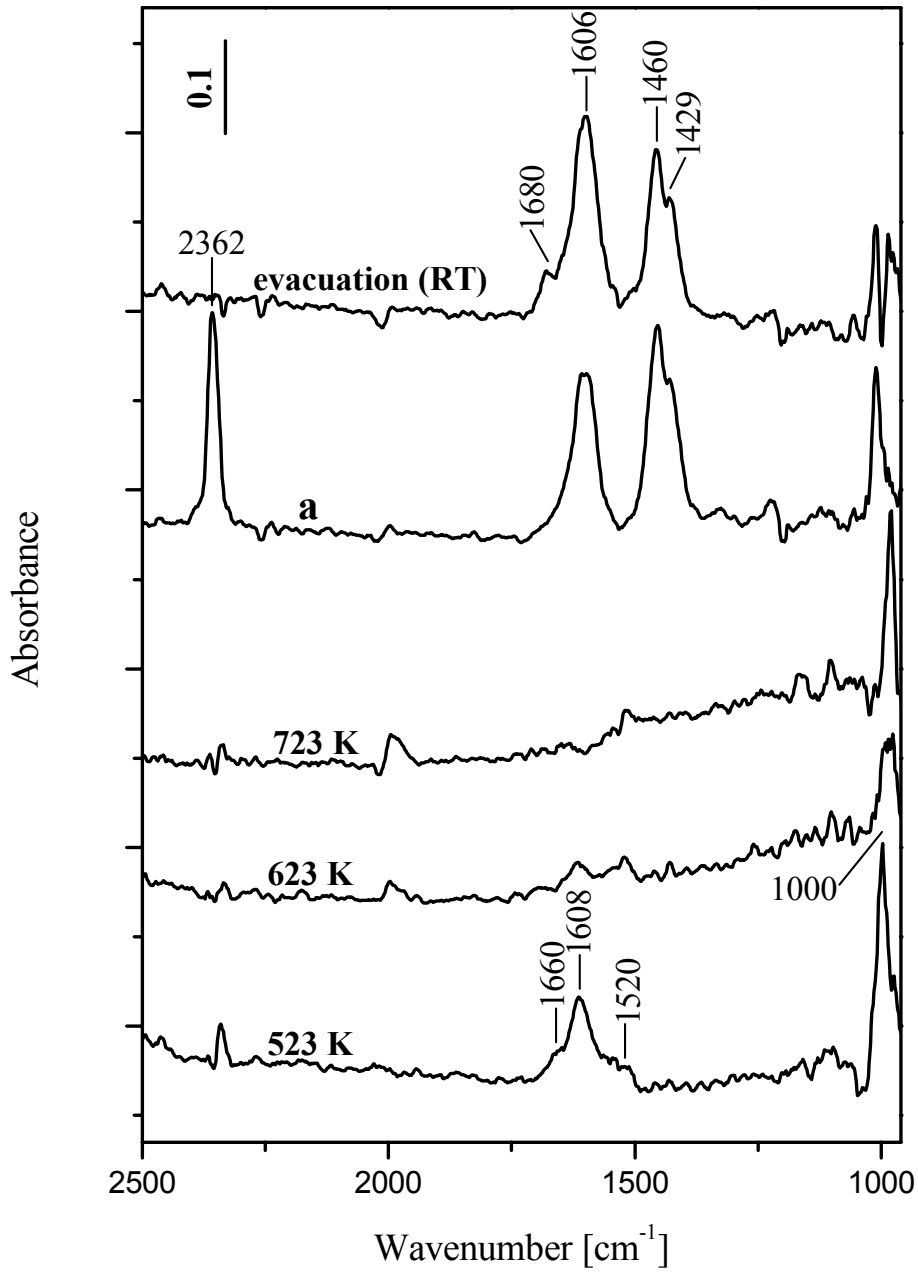

Figure 20. FT-IR spectrum of the WZ support taken after addition of methane (8 kPa) at room temperature, followed by heating of the closed IR cell for 20 min. Then cooling to RT (a). The spectrum of the activated sample is used as a background reference and the gas phase spectra are subtracted.

zirconia is unreducible below 900 K [79], the oxidation of methane can be caused by the oxide ions coordinated to the tungsten(VI) species. This results in perturbation of the wolframyl groups (positive absorption at 1000 cm^{-1}).

3. 3. 2. 2. With The Pd/WZ Catalyst

Heating of the activated Pd/WZ catalyst in the presence of methane (constant pressure of 8 kPa) in the temperature range 523 – 723 K results in appearance of bands similar to those detected on the WZ support. Noticeable difference is the higher thermal stability of the carbonates formed on the surface of the Pd/WZ catalyst: bidentate carbonate bands at 1560 and 1511 cm^{-1} are detected at 723 K. This can be due to coordination of the carbonate species to reduced palladium sites. As in the case of the WZ sample, the spectra obtained after cooling to room temperature (Fig. 21, spectrum a) and after evacuation (in Fig. 21) contain bands corresponding to bidentate (1600 cm^{-1}), monodentate (1454 and 1430 cm^{-1}) and hydrogen-carbonates (1640 and 1219 cm^{-1}). Since it is well known that Pd(II)-containing catalysts are very active in the complete oxidation of methane, it is reasonable to conclude that both Pd(II) and W(VI) are involved in this process.

Figure 22 compares the spectra of the WZ and the Pd/WZ taken from the blank CH_4 experiment after the final evacuation at room temperature. Fig. 22 indicates that the amount of the surface carbonates on the WZ is higher than that on the Pd/WZ.

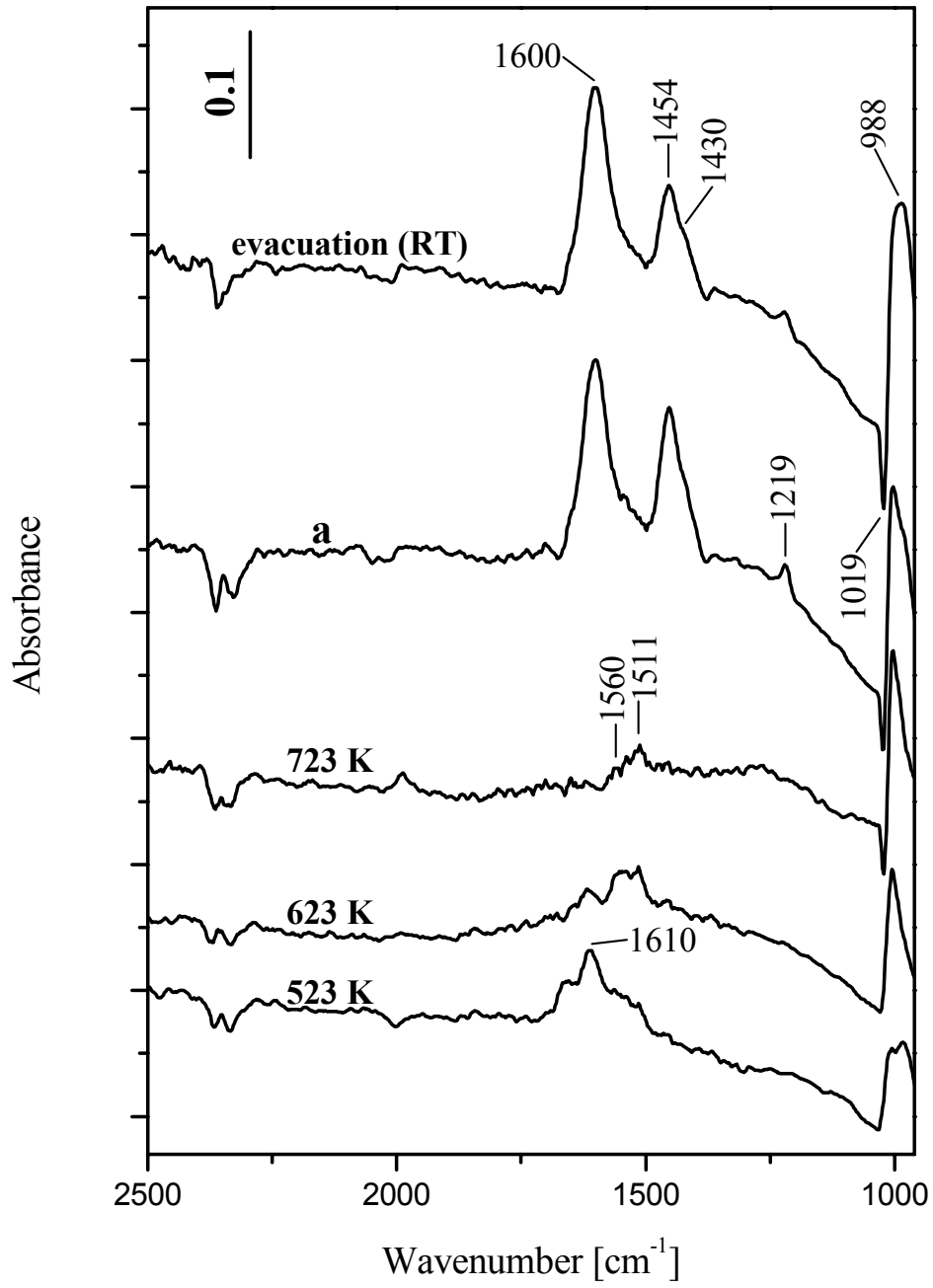

Figure 21. FT-IR spectrum of the Pd/WZ sample taken after addition of methane (8 kPa) at room temperature and followed by heating of the closed IR cell for 15 min. Then cooling to RT (a). The spectrum of the activated sample is used as a background reference and the gas phase spectra are subtracted.

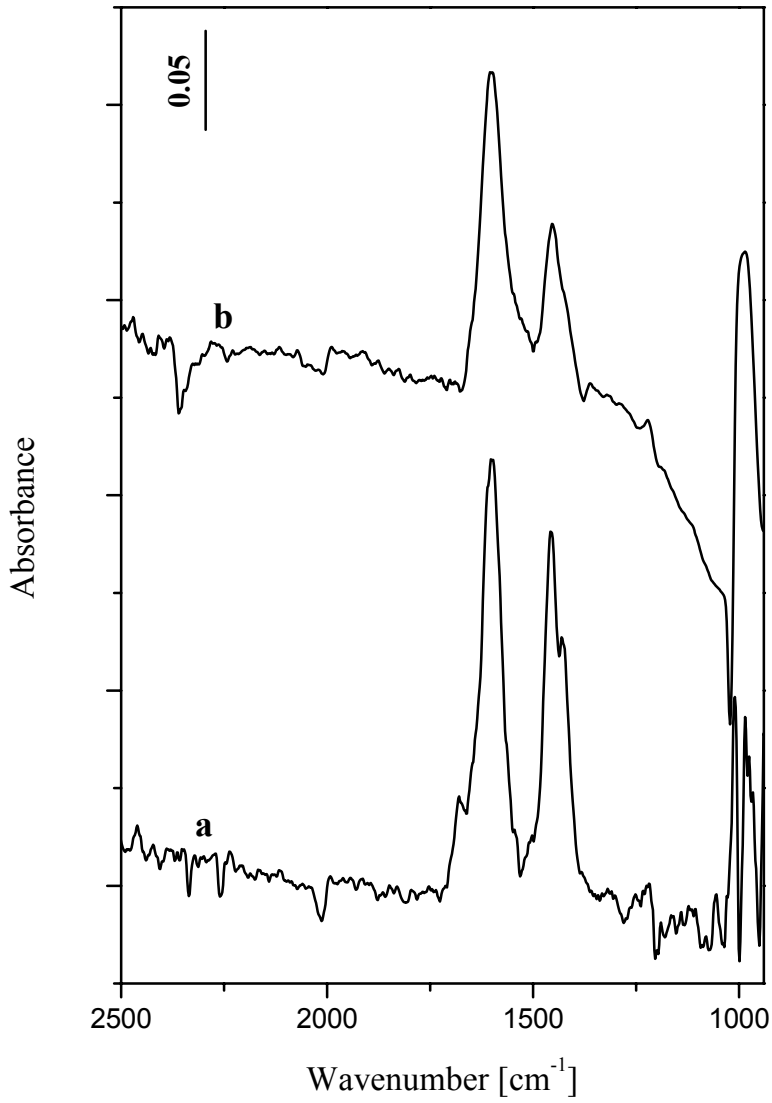

Figure 22. FT-IR spectra taken from "Blank CH_4" experiment after the final evacuation at room temperature for the WZ sample (a) and for the Pd/WZ sample (b).

3. 3. 3. Interaction of Preadsorbed NO_x species with Methane

3. 3. 3. 1. On The WZ Support

After the formation of NO_x species on the WZ support by room temperature adsorption of NO/O_2 followed by evacuation for 15 min (Fig. 23, spectrum a), methane (7.33 kPa) was added (Fig. 23, spectrum b). Then the closed

IR cell was heated in the 573 – 723 K temperature range. The spectrum taken at 573 K (Fig. 23, spectrum at 573 K) shows considerable decrease in the intensities of the nitrate bands and restoration of the perturbed W^{6+} = O groups (strong decrease in the intensity of the negative band at 1012 cm^{-1}). The positive band at 1000 cm^{-1} corresponds to the restored W^{6+} = O groups, which differ from the originally present. The increase in the temperature to 723 K leads again to perturbation of the wolframyl species (the negative band at 1012 cm^{-1} appears in the spectra from d to f with growing intensity). This can be explained by assuming that the tungsten(VI) ions, but not the NO_x species, are involved in the interaction with methane. The adsorbed NO_3^- species most probably block the active sites for methane oxidation and the oxidation process starts at 623 K, after the nitrates leave the surface. This temperature is by approximately 100 K higher than the temperature at which oxidation products of methane on the surface of the NO_x-free sample are detected (523 K, See Section 3.3.2.1, Fig. 20). The spectrum taken at room temperature (Fig. 23, spectrum c) contains bands, which can be assigned to bidentate (1602 cm^{-1}) and monodentate carbonates (1450 and 1420 cm^{-1}). The weak band at 2040 cm^{-1} can be attributed to CO adsorbed on W^{4+} ions [80]. The negative band at 2012 cm^{-1} is due to the overtone of the perturbed W^{6+} = O groups at 1010 cm^{-1}. It should be pointed out that, as in the case of the "Blank NO_x" experiment, the gas-phase spectrum does not contain NO_x species.

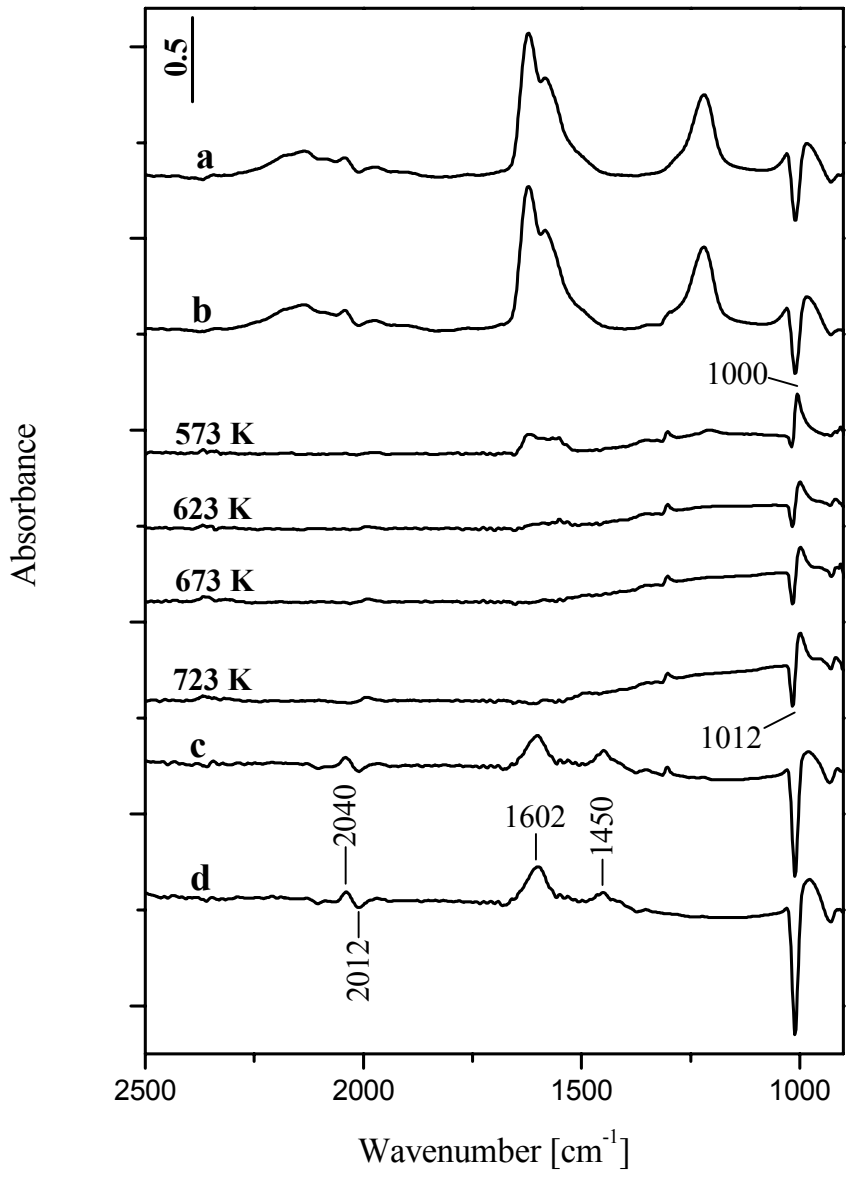

Figure 23. FT-IR spectra of the WZ support taken after adsorption of NO/O_2 mixture (1.33 kPa:2.66 kPa, $NO:O_2$ = 1:2) at RT followed by evacuation for 15 min (a) and addition of 7.33 kPa of CH_4 (b), after heating of the closed IR cell for 20 min and then cooling to RT (c), subsequently evacuation of the gas phase at RT (d). The spectrum of the activated sample is used as a background reference.

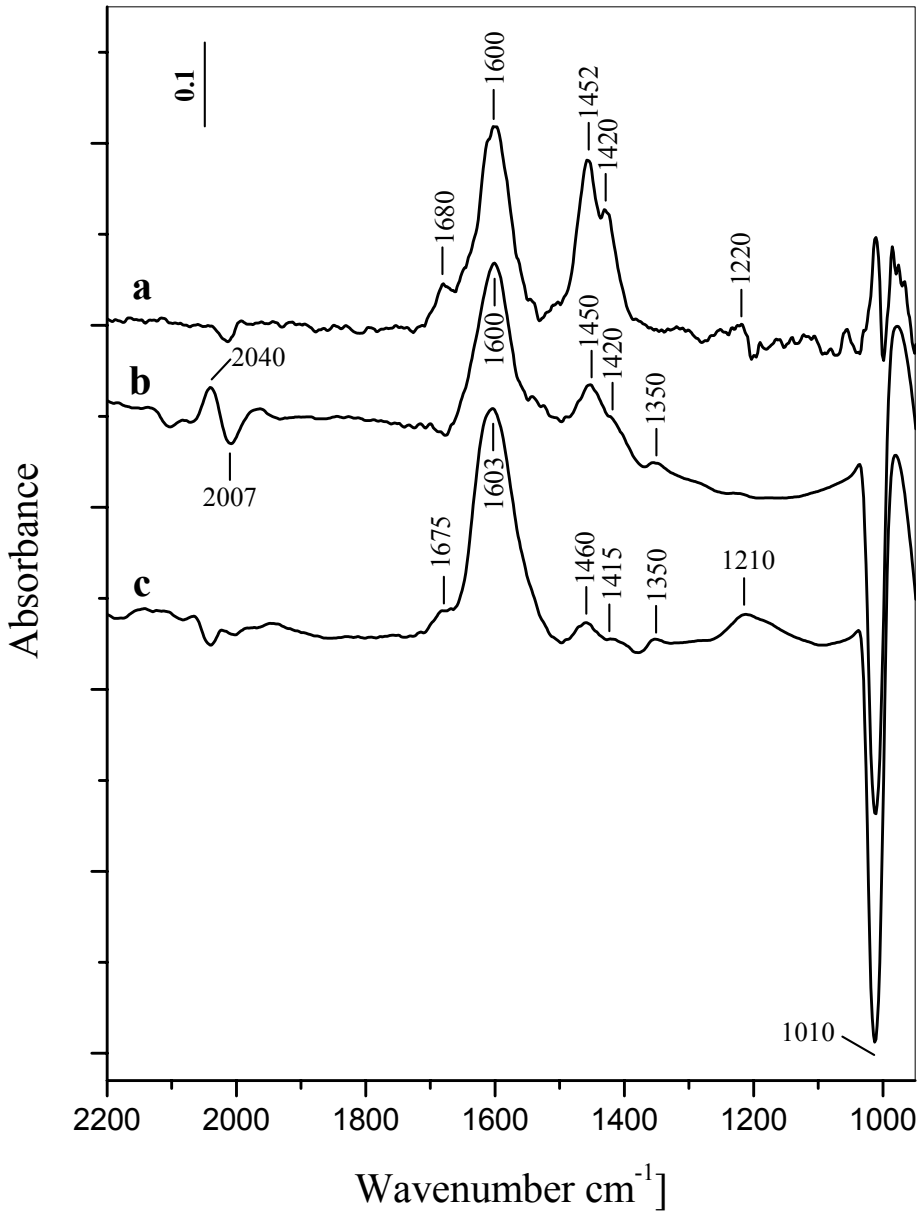

Figure 24. FT-IR spectra of the WZ support taken from the "Blank CH_4" (a), the interaction of the preadsorbed NO_x with CH_4 (b) and the "Blank NO_x" (c) experiments after the final evacuation at room temperature. The spectrum of the activated sample is used as a background reference.

Figure 24 compares the spectra of the WZ sample obtained in the "Blank CH_4" (spectrum a), "CH_4-NO_x" (spectrum b) and "Blank NO_x" (spectrum c) experiments after the final evacuation at room temperature (see Fig. 20, spectrum after evacuation at RT; Fig. 23, spectrum d; Fig. 18, spectrum d).

Intensities of the carbonate bands in spectrum b are lower than those in spectrum a. Moreover, by comparing spectra a and b it can be seen that the ratio of the intensities of the bands at 1600 cm^{-1} versus those at 1450 and 1420 cm^{-1} differs. The intensity of the band at 1600 cm^{-1} in spectrum b relative to those at 1450 and 1420 cm^{-1} is much higher. This difference can be explained by taking into account the spectrum c obtained in the "Blank NO_x" experiment. In absence of interaction between the methane and the surface nitrates relatively strong nitrate band at 1603 cm^{-1} is present in spectrum c. It can be assumed that the nitrate and bidentate carbonate bands in the spectrum b obtained in the "CH_4-NO_x" experiment are superimposed, which leads to enhancement of the intensity of the band at 1601 cm^{-1}. In addition, the spectrum from the "Blank CH_4" experiment taken at room temperature in the presence of the gas phase (Section 3.3.2.1, Fig. 20, spectrum d) contains sharp band at 2362 cm^{-1} corresponding to adsorbed CO_2. Under the same conditions, in the "CH_4-NO_x" experiment, no adsorbed CO_2 is detected (Fig. 23, spectrum c). These data clearly illustrate that the preadsorbed NO_x species on the surface of the tungstated zirconia suppress the oxidation of methane.

3. 3. 2. 2. On The Pd/WZ Catalyst

Stable NO_x species were created on the Pd/WZ sample as described in the previous section and then 7.33 kPa of CH_4 was added (Fig. 25, spectrum a).

The treatment at 473 K (Fig. 25(A), spectrum b) causes disappearance of the NO^+ species (broad absorption between 2250 and 2000 cm^{-1}), Pd(II) nitrosyls (1876 and 1824 cm^{-1}) and decomposition of the monodentate nitrates (unresolved bands at about 1500 and 1270 cm^{-1}). In the gas phase formation of NO_2 is detected (Fig. 25(C), spectrum b). Further increase in the temperature to 523 K (Fig. 25(A), spectrum c and Fig. 25(B), spectrum b-c) results in loss of the bridged (1647 and 1190 cm^{-1}) and bidentate (1590 and 1220 cm^{-1}) nitrates leading to additional increase in the amount of gaseous NO_2 (Fig. 25(C), spectrum c). The weak positive bands at 1542, 1435, 1380 (shoulder) and 1366 cm^{-1} in the subtraction spectrum b-c indicate formation of new species. At 573 K (Fig. 25(A), spectrum d) all of the surface nitrates have decomposed, which is evident by the absence of the band at 1200 cm^{-1} corresponding to the $\nu_{as}(NO_2)$ modes (see also the subtraction spectrum d-c in Fig. 25(B)). However, no further increase in the

amount of the gaseous NO_2 is detected (Fig. 25(C), spectrum d). In contrary, there is a strong decrease in the intensity of its IR band. This experimental fact leads to the conclusion that at 573 K NO_2 does not leave the surface. It is consumed for the formation of the new species, whose spectral features are clearly observed as positive bands at 1557, 1440, 1381 and 1357 cm^{-1} in the subtraction spectrum d-c (Fig. 25(B)).

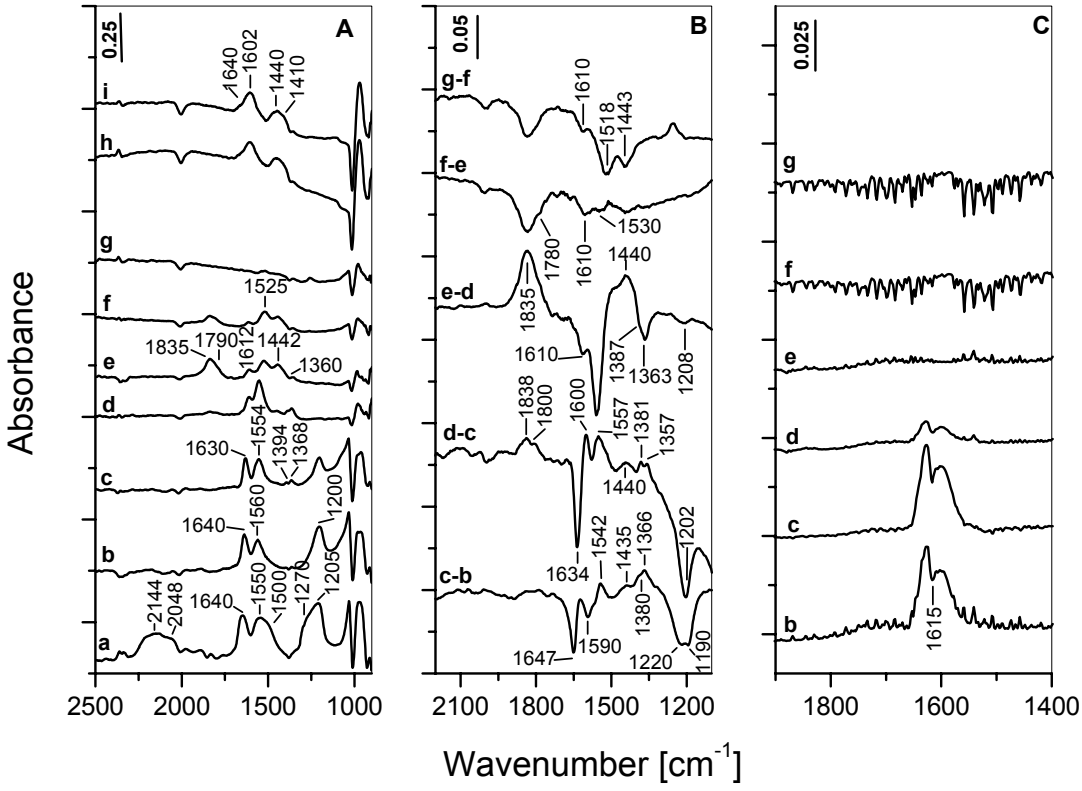

Figure 25. (A) FT-IR spectra of the Pd/WZ catalyst taken after adsorption of NO/O_2 mixture (1.33 kPa:2.66 kPa, $NO:O_2$ = 1:2) at RT followed by evacuation for 15 min and addition of 7.33 kPa of CH_4 (a), after heating of the closed IR cell for 15 min at 473 K (b), 523 K (c), 573 K (d), 623 K (e), 673 K (f), 723 K (g) and then cooling to RT (h), subsequently evacuation of the gas phase at RT (i). The spectrum of the activated sample is used as a background reference. (B) FT-IR subtraction spectra of the Pd/WZ catalyst obtained from the spectra shown in panel A. (C) Gas phase spectrum of the corresponding spectrum shown in panel A.

These bands cannot be assigned to inorganic NO_2^- (nitro) species produced by transformation of the adsorbed nitrates because in the "Blank NO_x" experiment with the Pd/WZ catalyst no such bands are detected (Section 3.3.1.2, Fig. 19). Based on literature data [53,56,57,80], the bands at 1557, 1440, 1381 and 1357 cm^{-1} are attributed to the $\nu_{as}(NO_2)$, $\delta_{as}(CH_3)$, $\nu_s(NO_2)$ and $\delta_s(CH_3)$ of adsorbed CH_3NO_2, respectively. The positive band at 1600 cm^{-1} is assigned to adsorbed NO_2 (see section high-temperature adsorption of NO). The weak band at 1838 cm^{-1} with shoulder at 1800 cm^{-1} present in the subtraction spectrum d-c increase significantly in intensity at 623 K (Fig. 25(A), spectrum e and 25(B), spectrum e-d). This is accompanied by decrease in the amount of adsorbed NO_2 (negative band at 1610 and 1208 cm^{-1}) and disappearance of the adsorbed nitromethane (negative bands at 1557, 1387 and 1363 cm^{-1}). Formation of new species (which will be identified below) exhibiting absorption bands at 1525, 1442 and 1360 cm^{-1} is detected (Fig. 25(A), spectrum e). The bands at 1835 and 1790 cm^{-1} (Fig. 25(A), spectrum e and Fig. 25(B), spectrum e-d) correspond to NO adsorbed on two different Pd(I) sites. Obviously, the adsorbed NO arises as a decomposition product of the nitromethane. The heating at 673 K (Fig. 25(A), spectrum f and Fig. 25(B), spectrum f-e) affects considerably the intensities of the Pd^+–NO nitrosyl bands. This decrease could be associated with interaction of the transformation product(s) with the adsorbed NO or its oxidation to NO_2. However, the latter process is not likely to occur because there is decrease in the intensity of the band at 1610 cm^{-1} (Fig. 25(A), spectrum f, Fig. 25(B), spectrum f-e). Rising the temperature to 723 K (Fig. 25(A), spectrum g) results in complete disappearance of all of the adsorption bands. The spectrum taken after cooling to room temperature displays bands, which fall in the carbonate-carboxylate region (Fig. 25, spectra h and i). Fig. 26 compares the results of the "NO_x-CH_4", "Blank CH_4" and "Blank NO_x" experiments. The spectra obtained after the interaction of the CH_4 with the NO_x-precovered and NO_x-free Pd/WZ catalyst are similar, which shows that the main products in both cases are adsorbed carbonate species.

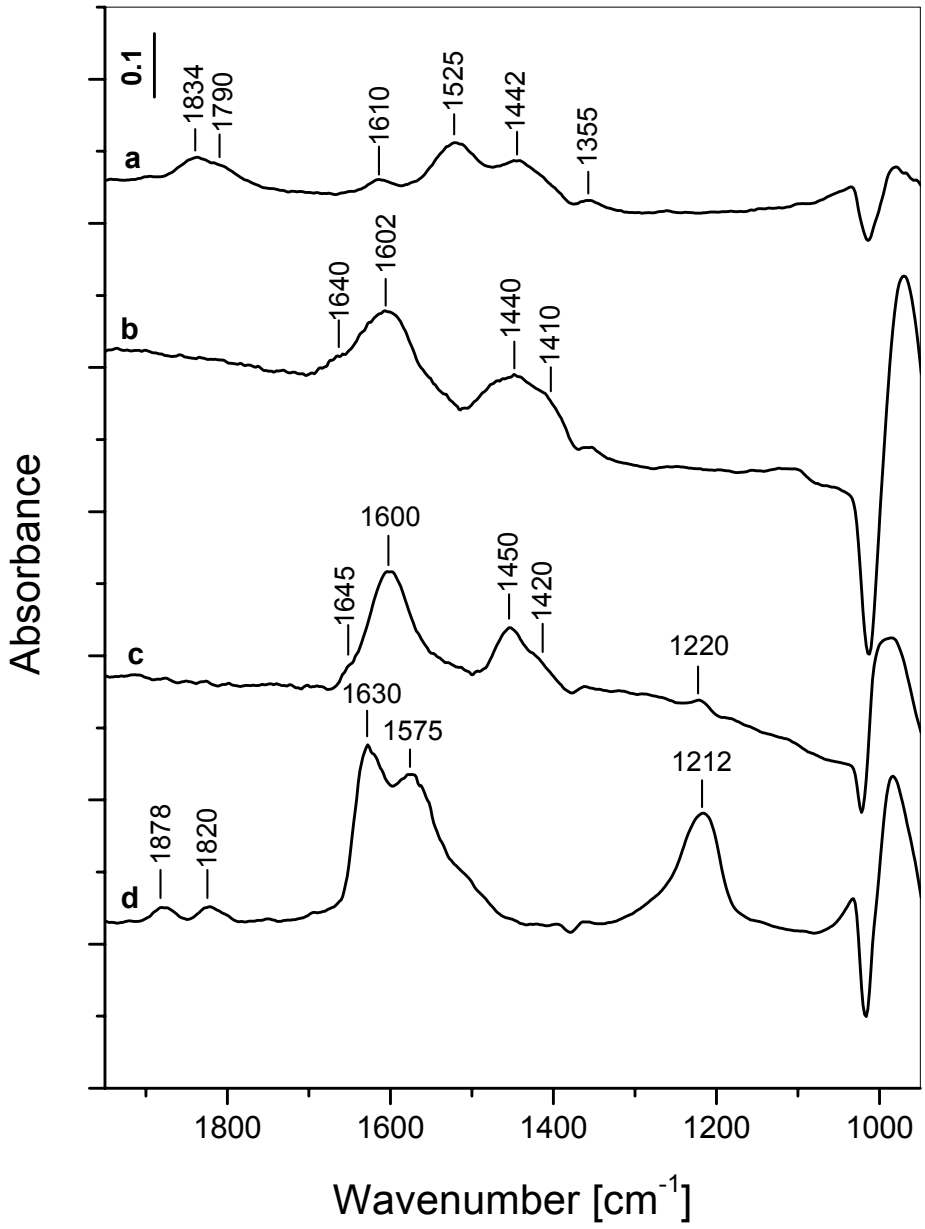

Figure 26. FT-IR spectra of the Pd/WZ catalyst taken from the interaction of the preadsorbed NO_x with CH_4 at 673 K (a) and after evacuation at room temperature (b), the "Blank CH_4" (c), and the "Blank NO_x" (d) experiments after the final evacuation at room temperature. The spectrum of the activated sample is used as a background reference.

3. 4. Summary of the Results on the Reactivity of the Adsorbed NO_x Species toward Methane

The experimental results show that the CH_4 interacts in a different way with the NO_x-precovered tungstated zirconia and Pd/WZ catalyst although both materials are able to activate the hydrocarbon at the same temperature in absence of adsorbed NO_x species. In the case of the WZ sample, the surface nitrates suppress the oxidation of methane, whereas the NO_x-precovered Pd/WZ sample catalyzes the formation of nitromethane.

Studies with oxide systems [82,83] have shown that methane is adsorbed dissociatively over strong Lewis acid-base pairs with generation of metal – alkyl and methoxy species. The following reaction steps can be proposed for the oxidation of the methane on the NO_x-free WZ sample:

$$CH_4 + WO^{4+} \rightarrow [W{-}CH_3]^{5+} + OH^- \quad (10)$$

$$[W{-}CH_3]^{5+} + O^{2-} \rightarrow W^{4+} + CH_3{-}O^- \quad (11)$$

$$CH_3{-}O^- + 3WO^{4+} \rightarrow HCO_3^- + H_2O + 3W^{4+} \quad (12)$$

$$HCO_3^- + O^{2-} \rightarrow CO_3^{2-} + OH^- \quad (13)$$

Scheme 1

It is assumed that steps from (10) to (12) are fast and therefore the methoxy species cannot be detected. This reaction scheme explains the negative effect of the preadsorbed NO_x species on the activity of tungstated zirconia in the oxidation of methane in absence of molecular oxygen. The nitrates formed by room-temperature adsorption of NO/O_2 do not interact with methane and block the wolframyl groups considered as active sites for the hydrocarbon activation.

In the case of the Pd/WZ catalyst, there are two kinds of sites that are candidates for methane activation: the Pd(II) and W(VI) species. Reaction scheme analogous to Scheme 1, in which Pd(II) ions are involved, could operate as well with a change in the oxidation states of palladium from +2 to zero. However, the introduction of palladium to the tungstated zirconia did not increase the conversion of methane in the "Blank CH_4" experiment. In contrary, the surface concentrations of the HCO_3^- and CO_3^{2-} produced on the Pd/WZ catalyst are lower than those on the tungstated zirconia (see Fig. 22).

Valyon et al. [83] proposed that if the CH_3^- groups cannot be stabilized by the oxide, $\bullet CH_3$ radicals can be produced. In the case of the Pd/WZ catalyst the following reactions can be assumed:

$$CH_4 + Pd^{2+}{-}O^{2-} \rightarrow [Pd{-}CH_3]^+ + OH^- \quad (14)$$

$$[Pd{-}CH_3]^+ \rightarrow Pd^+ + \bullet CH_3 \quad (15)$$

The $\bullet CH_3$ species following reaction (16) can convert back to methane:

$$\bullet CH_3 + Pd^+ + OH^- \rightarrow CH_4 + Pd^{2+}{-}O^{2-} \quad (16)$$

This process leads to decrease in the amount of the activated methane and can explain the lower conversion of the hydrocarbon on the Pd/WZ catalyst observed in absence of molecular oxygen compared to that on the WZ sample.

The formation of nitromethane on the NO_x-precovered Pd/WZ catalyst starts at 523 K. At this temperature the hydrocarbon is already activated on the NO_x-free catalyst: hydrogencarbonates and carbonates are detected indicating that the oxidation of the methane takes place in absence of molecular oxygen. It can be proposed that the $\bullet CH_3$ radicals, which are produced according to reaction (15) are captured by the NO_2 realized during the decomposition of the nitrate species (see Fig. 19, page 42):

$$\bullet CH_3 + NO_2 \rightarrow CH_3NO_2 \quad (17)$$

The IR data obtained during the interaction of CH_4 with the NO_x-precovered Pd/WZ catalyst show that at 623 K nitromethane transforms in the compound(s) characterized by the absorption bands at 1525, 1442 and 1360 cm^{-1} and NO adsorbed on Pd(I) sites (Fig. 25(A), spectrum e). The weak band at 1612 cm^{-1} belongs to adsorbed NO_2, which resists even the evacuation at 623 K as shown in Section 3.2.3. It can be proposed that the nitromethane undergoes reductive transformation according to the following reaction:

$$Pd^{2+}{-}O^{2-} + CH_3NO_2 \rightarrow Pd^+ + NO + OH^- + H_2C{=}O \quad (18)$$

The formaldehyde is unstable on oxide surfaces [84,85] and can be oxidized fast by the Pd(II) to formic acid:

$$H_2C{=}O + Pd^{2+}{-}O^{2-} \rightarrow HCOOH + Pd^o \quad (19)$$

The bands at 1525 and 1360 cm^{-1} (Fig. 25(A), spectra e and d) are assigned to the $\nu_{as}(CO_2)$ and $\nu_s(CO_2)$ stretching modes of bidentate formate ion [67,68,78], whereas the band at 1442 cm^{-1} most probably is due to monodentate carbonate [67]. The latter species can be formed either by decomposition of the formate

(reaction 20) or by oxidation of the $HCOO^-$ with the adsorbed NO and NO_2 (reactions 21):

$$HCOO^- + 2O^{2-} \rightarrow CO_3^{2-} + OH^- \quad (20)$$

$$HCOO^- + NO \rightarrow HCO_3^- + \tfrac{1}{2} N_2 \xrightarrow{O^{2-}} CO_3^{2-} + OH^- \quad (21)$$

$$2HCOO^- + NO_2 \rightarrow 2HCO_3^- + \tfrac{1}{2} N_2 \xrightarrow{2O^{2-}} 2CO_3^{2-} + 2OH^- \quad (22)$$

Oxidation of the formaldehyde by NO or NO_2 to formic acid and/or carbonates is not excluded. This assumption (reactions 21) is supported by the fact that the bands due to the formate species decrease in intensity at 673 K and disappear together with the adsorbed NO and NO_2 at 723 K. The carbonates at 1442 cm^{-1} desorb also at 723 K. After cooling to room temperature bidentate (1602 cm^{-1}) and monodentate carbonates (broad band with maximum at 1440 cm^{-1}) are detected. Some amount of hydrogencarbonates is observed as well (band at 1640 cm^{-1}). It should be pointed out that Beloshapkin et al. [56] reported also formation of adsorbed NO during the thermal transformation of nitromethane on Co-ZSM-5 at 553 K.

Sun et al. [52] first observed, by means of DRIFT, the formation of CH_3NO_2 on the Co-ZSM-5 and proposed this compound as an intermediate in the SCR of NO with CH_4 in presence of oxygen. Since then a vast amount of studies [54,55,85], mainly on zeolitic catalysts, is devoted to the investigation of the routes of nitromethane transformations to yield the products of the CH_4-SCR: N_2, CO_2 and H_2O. In general, the following overall scheme for Co-ZSM-5 as catalyst is widely accepted, which involves very fast steps of nitromethane transformation [54,55,86-88]:

$$CH_3NO_2 \rightarrow CO_2 + NH_3$$

$$CH_3NO_2 \rightarrow HNCO + H_2O$$

$$3HNCO + 3NH_3 \rightarrow C_3N_6H_6 + 3H_2O$$

The intermediate formation of ammonia, which is an efficient reducing agent of NO, can lead to the products of the SCR. Watson and Ozkan [51] observed formation of NH_3 during the interaction of $NO+O_2+CH_4$ mixture on Pd/TiO2 catalyst.

The final transformation product, the cyclic compound $C_3N_6H_6$ (melamine), is detected during the decomposition of nitromethane on Co-ZSM-5 at elevated temperatures giving rise to a sharp tailing band at 1662 – 1665 cm^{-1}

[56, 88]. No such a band is present in the spectra taken above 573 K in the case of the Pd/WZ catalyst. The melamine can be removed at 673 K by heating in oxygen [56].

The difference in the reactivity of the NO_x-precovered tungstated zirconia and Pd-containing tungstated zirconia toward methane lies in the ability of the Pd/WZ catalyst to stabilize adsorbed NO_2 to relatively high temperatures (573 – 623 K). According to the experimental results the highest concentration of NO_2 adsorbed on the Pd/WZ catalyst is reached at 573 K, after the complete decomposition of the surface nitrates. In the case of the tungstated zirconia, no adsorbed NO_2 is detected at temperatures higher than the room temperature and in absence of NO/O_2 mixture. According to the results of the "Blank NO_x" and "CH_4-NO_x" experiments with the WZ sample, the spectrum of the gas phase taken after the heating at 723 K does not contain gaseous NO_x species. This indicates that the nitrates formed on the tungstated zirconia follow decomposition route different from that on the Pd/WZ catalyst. Most probably the gas phase in the former case contains both NO and NO_2 in low concentrations, which cannot be measured under the conditions of the existing path length of the IR cell. However, heating the NO_x-precovered Pd/WZ catalyst in the 523 – 723 K temperature range causes release of significant amount of NO_2 in the gas phase, which readsorbs at room temperature producing surface nitrates (Section 3.3.1.2, Fig. 19, spectra a and evacuation at RT). It can be concluded that the role of the nitrate species adsorbed on the Pd/WZ catalyst is to provide high surface concentration of NO_2 at high temperatures, which can interact with the hydrocarbon producing nitromethane.

4. CONCLUSIONS

1. The structures of the tungstated zirconia and palladium(II) supported on tungstated zirconia have been studied by means of XRD and FT-IR spectroscopy. Tungstated zircona was prepared by coprecipitation of solutions of $ZrOCl_2.H_2O$ and ammonium metatungstate using polyvinyl alcohol as a template. According to the XRD the sharp peak at low angle ($2\theta = 1.8^0$) shows formation of a mesoporous phase in the sample. The presence of WO_x groups and the mesoporosity ensure 100% tetragonal phase and small crystallites (~ 5 nm). The sample has high surface area compared to samples synthesized by conventional impregnation techniques. The introduction of palladium(II) using solution of Pd(II) nitrate affect considerably the amount of the mesoporous phase. The FT-IR spectra of the activated tungstated zirconia and Pd/tungstated zirconia reveal presence of W^{6+}=O groups.

2. The adsorption of NO on tungstated zirconia at room temperature allows detection of coordinatively unsaturated Zr(IV) ions. The wolframyl groups oxidize the adsorbed NO to N_2O_3 and NO_2^- species. The spectrum of NO on Pd/tungstated zirconia reveals the presence of two types of Pd(II) sites. No exposed Zr(IV) ions are observed. The surface NO_x species (N_2O_3, nitro and nitrito ions) as in the case of tungstated zirconia, are produced by oxidation of NO with the wolframyl species and the palladium(II) is not involved. However, the latter can oxidize the adsorbed NO to NO_2 at 623 K.

3. Upon coadsorption of NO and O_2 at room temperature on the samples studied, various kinds of surface nitrates are observed differing in the modes of their coordination. The thermal stability of the nitrate species formed on both materials is comparable. However, the concentration of the surface nitrates is lower for the Pd-containing sample, which indicates that the NO_3^- species formed on the latter are coordinated to the support.

4. The NO_x-free tungstated zirconia and Pd/tungstated zirconia are able to activate the methane already at 523 K in absence of molecular oxygen. However, judging from the intensities of the oxidation products (hydrogencarbonates and carbonates) the conversion of the hydrocarbon is lower for the Pd-containing

sample. This difference is explained by assuming destabilization of the metal-alkyl complex produced by dissociative adsorption of the methane in the presence of Pd(II) and formation of CH_3 radicals, which can recombine with surface protons back to methane.

5. In absence of molecular oxygen, the preadsorbed surface nitrates have negative effect on the activity of tungstated zirconia in the oxidation of methane. They do not interact with the hydrocarbon and block the wolframyl groups considered as active sites for the hydrocarbon activation.

6. In the case of the Pd/tungstated zirconia, the CH_3 radicals produced during the direct activation of the methane by the catalyst are captured by the NO_2 realized by the decomposition of the nitrate species, thus producing nitromethane. The highest surface concentration of nitromethane is detected at 573 K, after the complete decomposition of the NO_3^- species. Increasing the temperature above 573 K causes transformation of the nitromethane to NO adsorbed on Pd(I) sites and partially oxidized hydrocarbon, most probably formaldehyde. The latter undergoes fast oxidation to formate species, which interact with the adsorbed NO giving the products of the CH_4-SCR of NO: N_2, CO_2 and H_2O.

7. The role of WO_3 as modifier of the zirconia is to create high surface acidity of the support needed for the activation of methane. The addition of palladium(II) insures sufficient amounts of CH_3 radicals and adsorbed NO_2 resulting in the formation of nitromethane, the intermediate of the SCR of NO with methane in the presence of Pd/tungstated zirconia.

5. REFERENCES

[1] R.J. Farrauto, R.M. Heck, *Appl. Catal. A*, **221** (2001) 443-457.

[2] V.I. Parvulescu, P. Grange, B. Delmon, *Catal. Today*, **46** (1998) 233-316.

[3] J.N. Armor, *Catal. Today*, **26** (1995) 99-105.

[4] http://herkules.oulu.fi/isbn9514269543/html/c299.html.

[5] M. Shelef, *Chem. Rev.*, **95** (1995) 209-225.

[6] M.D. Amiridis, T. Zhang, R.J. Farrauto, *Appl. Catal. B*, **10** (1996) 203-227.

[7] http://www.epin.ncsu.edu/apti/ol_2000/module6/nitrogen/control/control.htm.

[8] http://www.unitedconveyor.com/bulletins/SCR.htm.

[9] http://www.ecn.nl/sf/products/emission_reduction/removal.en.html.

[10] M.D. Fokema, J.Y. Ying, *Catalysis Reviews*, **43** (1&2), 1-29 (2001).

[11] Y. Li, J.N. Armor, *Appl. Catal. B*, **1** (1992) L3.

[12] Y. Li, J.N. Armor, *J. Catal.*, **150** (1994) 376.

[13] K. Yogo, M. Ihara, I. Terasaki, E. Kikuchi, *Chem. Lett.*, **229** (1993).

[14] Y. Li, J.N. Armor, *J. Catal.*, **145** (1994) 1.

[15] J.N. Armor, *Catal. Today*, **31** (1996) 191.

[16] E. Kikuchi, K. Yogo, *Catal. Today*, **22** (1994) 73.

[17] G. Karakas, J.M. Watson, U.S. Ozkan, *Catal. Commun.*, **3** (2002) 199-206.

[18] Y.-H. Chin, W.E. Alvarez, D.E. Resasco, *Catal. Today*, **62** (2000) 159-165.

[19] Y.-H. Chin, W.E. Alvarez, D.E. Resasco, *Catal. Today*, **62** (2000) 291-302.

[20] K.A. Bethke, M.C. Kung, B. Yang, M. Shah, D. Alt, C. Li, H.H. Kung, *Catal. Today*, **26** (1995) 169-183.

[21] C.J. Loughran, D.E. Resasco, *Appl. Catal. B*, **7** (1995) 113-126.

[22] K. Okumura, T. Kusakabe, M. Niwa, *Appl. Catal. B*, **41** (2003) 137-142.

[23] D. Pietrogiacomi, S. Tuti, M.C. Campa, V. Indovina, *Appl. Catal. B*, **28** (2000) 43-54.

[24] J. Pasel, V. Speer, C. Albrecht, F. Richter, H. Papp, *Appl. Catal. B*, **25** (2003) 105-113.

[25] W. Stichert, F. Schüth, S. Kuba, H. Knözinger, *J. Catal.*, **198** (2001) 277-285.

[26] C.R. Vera, J.C. Yori, J.M. Parera, *Appl. Catal. A*, **167** (1998) 75-84.

[27] K. Tanabe, *Mater. Chem. Phys.*, **13** (1985) 347.

[28] P.D.L. Mercera, J.G.V. Ommen, E.B.M. Doesburg, A.J. Burggraaf, J .R.H. Ross, *Appl. Catal.*, **57** (1990) 127-148.

[29] K.T. Jung, A.T. Bell, *J. Mol. Catal. A*, **163** (2000) 27-42.

[30] A. Bahamonde, S. Campuzano, M. Yates, P. Salerno, S. Mendioroz, *Appl. Catal. B*, **44** (2003) 333-346.

[31] G.K. Chuah, *Catal. Today*, **49** (1999) 131-139.

[32] G. Štefanić, S. Musić, B.Gržeta, S. Popović, A. Sekulić, *J. Phys. Chem. Solids*, **6-7** (1998) 879-885.

[33] V.I. Pârvulescu, H. Bonnemann, V. Pârvulescu, U. Endruschat, A. Rufinska, Ch.W. Lehmann, B. Tesche, G. Poncelet, *Appl. Catal. A*, **214** (2001) 273-287.

[34] O.V. Melzhyk, S.V.Prudius, V.V. Brei, *Micropor. Mesopor. Mater.*, **49** (2001) 39-44.

[35] Y. Zhao, W. Li, M. Zhang, K. Tao, *Catal. Commun.*, **3** (2002) 239-245.

[36] V. Bolis, G. Cerrato, G. Magnacca, C. Morterra, *Thermochimica Acta*, **312** (1998) 63-77.

[37] C. Morterra, G. Cerrato, F. Pinna, M. Signoretto, *J. Phys. Chem.*, **98** (1994) 12373-12381.

[38] E. Zhao, Y.Isaev, A. Sklyarov, J.J. Fripiat, *Catal. Lett.*, **60** (1999) 173-181.

[39] M. Hino, K. Arata, *J. Chem. Soc. Chem. Commun.*, (1987) 1259.

[40] N. Naito, N. Katada, M. Niwa, *J. Phys. Chem. B*, **103** (1999) 7206-7213.

[41] D. Gazzoli, M. Valigi, R. Dragone, A. Marucci, G. Mattei, *J. Phys. Chem. B*, **101** (1997) 11129-11135.

[42] D.G. Barton, M. Shtein, R.D. Wilson, S.L. Soled, E. Iglesia, *J. Phys. Chem. B*, **103** (1999) 630-640.

[43] J.G. Santiesteban, J.C. Vartuli, R.D. Bastian, C.D. Chang, *J. Catal.*, **168** (1997) 431-441.

[44] M. Scheithauer, R.K. Grasselli, H. Knözinger, *Langmuir*, **14** (1998) 3019-3029.

[45] W. Ji, J. Hu, Y. Chen, *Catal. Lett.*, **53** (1998) 15-21.

[46] K. Shimizu, T.N. Venkatraman, W. Song, *Appl. Catal. A*, **224** (2002) 77-87.

[47] K. Okumura, T. Kusakabe, M. Niwa, *Appl. Cat. B*, **41** (2003) 137-142.

[48] L.J. Lobree, A.W. Aylor, J.A. Reimer, A.T. Bell, *J. Catal.*, **181** (1999) 189-204.

[49] K. Shimizu, F. Okada, Y. Nakamura, A. Satsuma, T. Hattori, *J. Catal.*, **195** (2000) 151-160.

[50] D.B. Lukyanov, E.A. Lombardo, G.A. Sill, J.L. d'Itri, W.K. Hall, *J. Catal.*, **163** (1996) 447-456.

[51] J.M. Watson, U.S. Ozkan, *J. Mol. Catal. A*, **192** (2003) 79-91.

[52] T. Sun, M.D. Fokema, J.Y. Ying, *Catal. Today*, **33** (1997) 251-261.

[53] C.L. Levoguer, R.M. Nix, *J. Chem. Soc.,Faraday Trans.*, **93**(9) (1997) 1813-1820.

[54] A. Satsuma, A.D. Cowan, N.W. Cant, D.L. Trimm, *J. Catal.*, **181** (1999) 165-169.

[55] E.A. Lombardo, G.A. Sill, J.L. d'Itri, W.K. Hall, *J. Catal.*, **173** (1998) 440-449.

[56] S.A. Beloshapkin, E.A. Paukshtis, V.A. Sadykov, *J. Mol. Catal. A*, **158** (2000) 355-359.

[57] S. Kameoka, T. Chafik, Y. Ukisu, T. Miyadera, *Catal. Lett.*, **51** (1998) 11-14.

[58] K. Shimizu, A. Satsuma, T. Hattori, *Appl. Catal. B*, **25** (2000) 239-247.

[59] K.I. Hadjiivanov, *Catal. Rev.-Sci. Eng.*, **42**(1&2) (2000) 71-144.

[60] K. Nakamoto, "Infrared and Raman Spectra of Inorganic and Coordination compounds" Part B, 5th edition, Wiley, New York, **1997.**

[61] M. Kantcheva, E.Z. Ciflikli, *J. Phys. Chem. B*, **106** (2002) 3941-3949.

[62] S.J. Huang, A.B. Walters, M.A. Vannice, *J. Catal.*, **192** (2000) 29-47.

[63] V.A. Sadykov, V.V. Lunin, V.A: Matyshak, E.A. Paukstis, A. Ya. Rozovski, N.N. Bulgakov, J.R.H. Ross, *Kinetics and Catalysis*, **44**(3) (2003) 379-400.

[64] P.D.L. Mercera, J.G. Van Ommen, E.B.M. Doesburg, A.J. Burggraaf, J.R. Ross, *Appl. Catal.*, **57** (1990) 127.

[65] H.P. Klug, L.E. Alexander, *X-Ray Diffraction Procedures*, Wiley, New York, 1974.

[66] D.G. Barton, S.L. Soled, G.D. Meitzner, G.A. Fuentes, E. Iglesia, *J. Catal*., **181** (1999) 57-72 .

[67] M. Valigi, D. Gazzoli, I. Pettiti, S. Colonna, S. De Rossi, G. Ferraris, *Appl. Catal. A*, **231** (2002) 159-172.

[68] K.T. Jung, A.T. Bell, *J. Mol. Catal. A: Chem.*, **163** (2000) 27-42.

[69] H. Toraya, M. Yoshimura, S. Somiya, *J. Am. Ceram. Soc.*, **67** (1984) C119-C128.

[70] G. Busca, V. Lorenzelli, *Mater. Chem.*, **7** (1982) 89-126.

[71] V. Bolis, G. Magnacca, G. Cerrato, C. Morterra, *Top. Catal.*, **19** (2002) 259.

[72] G. Ramis, G. Busca, C. Cristiani, L. Lietti, P. Forzatto, F. Bregani, *Langmuir*, **8** (1992) 1744.

[73] G. Busca, *Catal. Today*, **41** (1998) 191.

[74] J. Laane, J.R. Ohlsan, *Prog. Inor. Chem.*, **1986**, 28, 465.

[75] N. Macleod, R. Cropley, J.M. Keel, R.M. Lambert, *J. Catal*., **221** (2004) 20-31.

[76] P. Vijayanand, K. Chakarova, K. Hadjiivanov, P. Lukinskas, H. Knözinger, *Phys. Chem. Chem. Phys.*, **5** (2003) 4040-4044.

[77] M. Kantcheva, V.P. Bushev, K.I. Hadjiivanov, *J. Chem. Soc.,Faraday Trans.*, **88**(20) (1992) 3087-3089.

[78] M. Kantcheva, V.P. Bushev, K.I. Hadjiivanov, C. Klissurski, *Langmuir*, **10** (1994) 464-471.

[79] G. Delahay, E.E. Ensuque, Coq and F. Figueras, *J. Catal*., **175** (1998) 7-15.

[80] J.R. Hill, D.S. Moore, S.C. Schmidt, C.B. Storm, *J. Phys. Chem.*, **95** (1991) 3037-3044.

[81] S.D. Kohler, J.G. Ekerdt, *J. Phys. Chem.*, **98** (1994) 1276.

[82] R. Burch, D. J. Crittle, M. J. Hayes, *Catal. Today*, **47** (1999) 229.

[83] Valyon, J., Engelhardt, J., Kalló, D., and Hagedüs, M., *Catal. Lett.* **82**, 29 (2002).

[84] G. J. Millar, C. H. Rochester, K. C. Waugh, *J. Chem. Soc. Faraday Trans.*, **87** (1991) 2785.

[85] M. Kantcheva A. S. Vakkasoglu, *J. Catal*., 223 (2004) 364-371.

[86] N.W. Cant, A.D. Cowan, I.O.Y. Liu, A. Satsuma, *Catal. Today*, **54** (1999) 473.

[87] N.W. Cant, D.C. Chambers,A.D. Cowan, I.O.Y. Liu, A. Satsuma, *Top. Catal.*, **10** (2000) 13.

[88] A.D. Cowan, N.W. Cant, B.S. Haynes, P.F. Nelson, *J. Catal.*, **176** (1998) 329.